TWENTY FIRST CENTURY PROJECTIONS OF EXTREME PRECIPITATIONS IN THE PLATA BASIN

Journal:	*The International Journal of River Basin Management*
Manuscript ID:	JRBM-2013-0014
Manuscript Type:	Special Issue Paper
Date Submitted by the Author:	05-Feb-2013
Complete List of Authors:	Barros, Vicente Garavaglia, Christian; CONICET/UBA-UMI-IFAECI, CIMA; Servicio Meteorologica Nacional, Doyle, Moira; CONICET/UBA - UMI-IFAECI, CIMA; Universidad de Buenos Aires, Dto Ciencias de la Atmósfera y los Océanos
Keywords:	Climate Change, La Plata Basin, floods, twenty first century

TWENTY FIRST CENTURY PROJECTIONS OF EXTREME PRECIPITATIONS IN THE PLATA BASIN

Vicente R. Barros [1, 2]

Christian R. Garavaglia [1, 3]

and

Moira E. Doyle [1, 2]

[1] **Centro de Investigaciones del Mar y la Atmósfera (CIMA/CONICET-UBA) – UMI-IFAECI**

[2] **Departamento de Ciencias de la Atmósfera y los Océanos. Universidad de Buenos Aires**

[3] **Servicio Meteorológico Nacional**

FEBRUARY 2013

Corresponding Author:
Moira Doyle
Dto. Cs. De la Atmósfera y los Océanos
Ciudad Universitaria. Pabellón II, 2do piso
1428. Buenos Aires. Argentina
tel: (+54 11) 4576-3398
fax: (+54 11) 4576-3356
e-mail: barros@cima.fcen.uba.ar
garavaglia@cima.fcen.uba.ar
doyle@cima.fcen.uba.ar

ABSTRACT

Distributions of monthly rainfall averaged spatially over three regions of the Plata Basin (LPB) were projected for 2011-2040 and 2071-2100 using outputs of four regional climate models (RCMs) nested in three different general circulation models, run with the SRES A1B emission scenario. Tuning of simulations with observations was done at the control period 1981-1990.

During the past 50 years, in part of LPB there was a positive trend in annual precipitation. Two of the models indicate the maintenance of this trend over the northeast of Argentina and south of Brazil, while over the southernmost region of LPB, all models show growing precipitation throughout the 21st century. Trends are less ambiguous for extreme precipitation, especially in the southernmost part of LPB, where huge and long-lasting floods take place over plains with small drainage.

Months with extreme precipitation in LPB present a pronounced annual cycle with higher frequency from October to April. According to the RCM projections this pattern would persist during the twenty first century. Although, other factors cannot be discarded, the projected trends towards higher extreme monthly precipitation seem to be caused by an increase of the moisture convergence in the lower atmosphere over the east of LPB.

Key Words: *Climate Change, La Plata Basin, floods, twenty first century.*

1. INTRODUCTION

La Plata Basin (LPB), which stretches over 3 million km^2, is the fifth largest basin in the world and the second in South America. It is the core of the economic activities of Brazil, Uruguay and Argentina and includes all Paraguay. LPB population is near 130 million, and according to projections could reach 200 million by 2050 increasing the already important exposure of people, infrastructure and services to extreme precipitations and floods.

Long lasting floods in LPB can be characterized by two major types, namely overflows over banks of the big rivers and water excess stagnation on flat areas with very small runoff. The first type, which affects huge areas of the flood valleys of the Paraguay River, the Paraná River in Argentina and the Uruguay River, in extreme cases reaching 50,000 Km^2, are generally originated far upstream by great monthly or seasonal extended rainfalls in the middle of the LPB between 24° and 28 °S (Camilloni and Barros 2003, Barros *et al.* 2004).

The second type of long lasting floods takes place over very flat lands with slow drainage, mainly in the southern part of LPB in Argentina, and it is a distinctive feature of the regional hydrology (Latrubesse and Brea 2009). From now on, we will refer to them as plain floods. They range from a few to several hundred kilometres and in some cases last many months or even more than a year. The water excess is not only determined by rainfall immediately before the flood, but by other factors such as soil moisture where saturation may be reached as the result of either intense rainfall in a short period of time or by above normal precipitations over several months; also on evaporation and surface runoff, which are highly dependent on land cover and topography. Therefore it is difficult to find a direct simple relationship between floods and local or regional rainfall. However, in most of the largest floods of the last three decades, the mean regional precipitation exceeded the mean plus one standard deviation in the month when the flood starts. (Garavaglia *et al.* 2012) and therefore monthly precipitation over this threshold could be seen as indicative of potential flooding.

Both types of floods have become more frequent in the last decades. The main LPB rivers not only increased their mean discharges (García and Vargas 1998, Genta *et al.* 1998, Barros *et al.* 2004), but also the frequency of their extreme flows resulting in more frequent floods (Camilloni and Barros 2003, Barros *et al.* 2004). Regarding plain floods, there is a lack of systematic information to address the issue of trends in flooding; however these floods seem to have become more frequent after the 1980s. For example, the great flood events in what is known as the depression of the

Salado basin in the southernmost part of LPB have recurred almost every 10 years since the late 1980s, namely in 1987, 2001-2002 and 2012-2013.

These trends in flooding were matched with increased precipitation trends. Several authors have found positive precipitation trends which lead towards more humid conditions in South Eastern South America (SESA) during the second half of the 20th century (Castañeda and Barros 1994, Barros *et al.* 2000, Giorgi 2002, Liebmann *et al.* 2004, Haylock *et al.* 2006). Regarding the trends in extremes at a scale compatible with the long lasting regional floods, Doyle *et al.* (2012) showed a decrease in the frequency of months with low precipitation (below the 10th percentile), but an increase in the frequency of months with precipitation extremes (above the 90th percentile) that largely explain the mean annual positive precipitation trends over SESA. Extreme daily rainfall events in SESA, which favour small but particularly intense floods, also had a positive trend in recent years (Re and Barros 2009, Penalba and Robledo 2009).

Given the connection between extreme monthly precipitation and floods, the question that arises is if the positive trends in the frequency of extreme monthly precipitation will persist during the rest of this century or on the contrary will be irrelevant or even reversed. To address this issue, we may relay on the projections of Global Climate Models (GCMs) which are the most accepted tool for the characterization of future climate scenarios. However, they are deficient in adequately representing some observed regional features; in particular, they largely underestimate mean annual precipitation in the LPB (Boulanger *et. al.* 2007, Vera and Silvestri 2009, Saurral 2010). On the other hand, several authors point out that some variables related to precipitation, such as the atmospheric circulation or water vapour transport and convergence of humidity at low levels, are however well simulated by GCMs. In this sense, Solman and Le Treut (2006) found that the modelled EOF patterns of monthly 500 hPa geopotential heights anomalies compare reasonably well with those from the NCEP reanalysis Data for 1950–2000, while Gulizia *et al.* (2012), concluded that the overall pattern of water vapour transport and convergence in South America are also properly represented by GCMs. Garavaglia *et al.* (2012) found that there is a significant increase in the probability of occurrence of extreme monthly rainfall on the SESA when there are persistent conditions in the mid tropospheric levels of cyclonic vorticity advection and inflow of humidity in low levels coming from the north. Therefore, if precipitation projections by climate models result consistent with projections of circulation features and humidity advection, this consistency could be an additional source of confidence in the assessment of future precipitation fields.

Some, but not all GCM deficiencies in representing the observed precipitation field may be due to their low spatial resolution. To address this issue, it can be used regional climate models (RCMs) with higher spatial resolution, which may resolve certain regional scale features which GCMs are not able to properly depict. Even so, improved model resolution alone is insufficient to provide a quality simulation of South American climate (Seth *et al*. 2007) and a correction scheme should be applied to obtain acceptable future scenarios.

The main objective of this paper is to assess if large scale precipitation extremes aggregated at monthly scale, which sometimes result in extended floods in LPB, will continue to increase or become more frequent or not during the twenty first century. To this purpose, it was used climate projections of four RCMs nested in three different GCMs, which were run in the context of CLARIS LPB Project, a Europe-South America Network Collaborative Project for Climate Change Assessment and Impact Studies in La Plata Basin. These RCM models present systematic errors in describing the observed precipitation fields, which were calculated and then used to correct future precipitation scenarios over large LPB regions. In addition, to increase confidence in these projections, it was also analyzed to what extent the known main atmospheric drivers of heavy extended regional rainfall in the RCM projections have consistent trends with their extreme regional precipitation projections.

2. DATA

Simulated monthly precipitation, monthly geopotential height at 500 hPa level, daily specific humidity and zonal and meridional wind components at 1000, 900, 850 and 700 levels were taken from four RCMs for 3 different periods: 1981-1990 (control period), 2011-2040 (near future) and 2071-2100 (end of century).

The RCMs used were the Rossby Centre RCM version 3.5 (RCA), (Kjellström *et al.* 2005, Samuelsson *et al.* 2006) run with ECHAM5 GCM boundary conditions and 0.5x0.5º horizontal resolution, Prognostic at the Mesoscale version 2.4 (PROMES), (Sanchez *et al.* 2007, Dominguez *et al.* 2010) with HadCM3 GCM-Q0 boundary conditions and resolution of 50x50km, ICTP Regional Climate Model version 3 (RegCM3), (Pal *et al.* 2007, Da Rocha *et al.* 2009a,b) also with same boundary conditions and horizontal resolution, and Modele de Circulation Generale du LMD version 4 (LMDZ) (Hourdin *et al.* 2006, Li 1999) using GCM IPSL boundary conditions and 0.48º

of resolution approximately. All models run for the twenty first century with only one emission scenario, namely the SRES A1B, which is an intermediate scenario between possible very high and very low emission scenarios for this century.

Observed monthly rainfall from 60 stations distributed over southern and eastern LPB were taken from the Argentine National Weather Service, the Agência Nacional de Águas (ANA) and National Weather Service of Brazil, the National Weather Direction of Uruguay and the Direction of Meteorology and Hydrology of Paraguay, Fig 1. Tropospheric variables of the control period were taken from the global National Centers for Environmental Prediction-National Center for Atmospheric Research (NCEP–NCAR) reanalysis (Kalnay *et al*. 1996).

3. METHODOLOGY

3.1 Regions and indexes

The areal average of the observed monthly precipitation was calculated in three regions of LPB, R1, R2, and R3, Fig 1, for the observed period (1990-2004) and similarly for each RCM outputs for the control, near future and end of century periods.

Each of the three regions has nearly homogeneous features in the precipitation field with small gradients and similar annual regime and has a connection with long lasting floods. Region R1, includes southern Paraguay, most of north-eastern Argentina, and the western part of southern Brazil. The eastern region, R2, encompasses part of southern Brazil. The northern parts of these two regions are the main source of floods in the Paraguay and Paraná rivers (Camilloni and Barros 2003, Barros *et al.* 2004), while the southern part of R2 contributes to some of the major floods in the Uruguay River. R3 includes south-western Uruguay and most of the central-eastern Argentina, a region where most of the plain floods in LPB take place.

Regional averages of monthly precipitations will be considered extreme when they exceed their mean value plus one standard deviation; assuming a normal distribution for the sake of simplicity, this criterion implies that monthly regional averages are considered extreme when exceeding the percentile 83.5, which corresponds to approximately 200 mm. in regions 1 and 2 and 137 mm. in region 3. Based on these thresholds, the months of extreme precipitation (MEP) were determined for the observed and projected periods.

For almost the same three regions, Garavaglia *et al.* (2012) found important increments in the probabilities of occurrence of a MEP when thresholds of a few indexes were surpassed. These indexes describe circulation features over SESA and will be used here to assess if projections of extreme precipitation by the RCMs are consistent with their circulation projections.

To capture prevailing and persistent conditions of cyclonic vorticity advection over SESA, the index I500 is calculated from monthly 500 hPa geopotential as:

$$I500_i = (\overline{\varphi_{2_i}} - \overline{\varphi_{1_i}}) \quad (1),$$

where **i** denotes month, 1 and 2 correspond to the areas in the latitudinal band between 25° and 45° S over the South American continent (80°-60° W) and the Atlantic Ocean (50°-30° W) respectively; **φ** is geopotential height at 500hPa and the bar indicates areal average values. I500 higher values are consistent with the presence of a trough in the mid troposphere over the west of the South American continent at subtropical latitudes.

The two other indices used here were monthly means of the divergence of daily water vapor transport integrated between surface and 700hPa, west (DW) and east (DE) of 60º W, from latitudes 25° to 35° S between 65° and 60° W in the case of *DW* and between 60° and 50° W for DE.

3.2 Statistical distributions for the control period

3.2.1 Precipitation distribution

For each region, percentile distributions were calculated for the simulated regional monthly precipitation series and indices, and contrasted with the observations in the control period. RCMs underestimate the regional averages of monthly precipitation for all percentiles in the three regions, Figure 2. The only exception is the LMDZ model in region R2; this model is the one that less underestimates precipitation in the three regions. The highest discrepancies between simulated and observed precipitations in regions R1 and R3, are in the high and extreme monthly precipitation ranges reaching differences between 50 and 150 mm, which evidences the low skill of the RCMs to characterize extreme rainfall over SESA. In R2 the underestimation is approximately constant throughout the whole range, but still important. This general underestimation calls for some correction scheme in the projections of these models to obtain credible estimates of future precipitation scenarios.

3.2.2 Circulation index distributions

To explore the possible causes of the precipitation underestimation, it is also presented the percentile distribution of the circulation indices as calculated from the RCM simulations and compared with their respective observed distributions. In the case of the I500 index, Figure 3, positive (negative) values indicate prevailing cyclonic (anticyclonic) advection over SESA. Garavaglia *et al*. (2012) using an almost equivalent index found that when this index was above the threshold of 20 hPa there was a considerable increase in the probability of a MEP with respect to the climatologic value. Except in the case of the PROMES model, the percentage of the months with prevailing cyclonic advection in the observed case, about 30 %, was approximately similar in the other RCM simulations (Fig. 3). I500 values associated with prevailing anticyclonic advection were very well represented by these three models. RegCM3 model has the best representation of the circulation conditions that favour extreme rainfalls over SESA (high I500 percentiles), while RCA and LMDZ overestimate these conditions attaining the 20 hPa threshold with little more frequency than in the observations. Therefore, except for the case of PROMES, the underestimation of precipitation by RCMs in its whole percentile range including the highest values cannot be attributed to a model misrepresentation of the mid tropospheric circulation. Thus, these RCMs make a correct representation of a key feature of the circulation field for the development of precipitation in SESA. This result is consistent with the adequate GCM representation of the tropospheric circulation found by Solman and Le Treut (2006), since RCMs are nested in GCMs and presumably share with them their large scale atmospheric features.

The convergence of water vapour over the eastern region represented by the DE index is in general correctly captured by the RCMs, Figure 4, with the exception of the LMDZ model that indicates net convergence of moisture in almost every month of the period. In the extreme monthly events of moisture convergence (low percentiles), the RCA model tends to slightly underestimate this convergence while PROMES overestimates it; the RegCM3 model is the closest to observations. The thresholds in the convergence values that are related to a probability of a MEP higher than the climatic ones depend on the region ranging from -1 to -3 10^{-5} mms^{-1} in R1 and R2 respectively Garavaglia *et al*. (2012). With the exception of the LMDZ model, in general, these thresholds are attained by the model simulations in a percentage of months similar to the observed case.

Figure 5 shows the poor performance of the RCMs in representing the DW index during the control period. The observations indicate a preponderance of monthly cases with net convergence in this region, while three of the four models indicate only a few cases of net convergence with small values. The RegCM3 model distribution includes months, with net convergence or divergence but

also tend to underestimate the convergence with respect to observations. In conclusion, extreme months of moisture convergence in large region of western Argentina (low percentiles in DW) that favour extreme precipitations over SESA are poorly represented by the four RCMs.

Although the DW index represents the convergence of water vapour outside of the regions where precipitation is here studied, namely to the west, it has a considerable influence in the probability of occurrence of a MEPs on these regions when it is below the threshold of -4 to -5 10^{-5} mms^{-1} (Garavaglia *et al.* 2012). This is because most of the mesoscale convective systems (MCSs) that affect the southern LPB originate west of 60° W (Doyle *et al*., 2012) and then move eastwards (Salio *et al.,* 2007) where they reach a mature state and are responsible of pouring rainfalls that account for about 60% of the annual precipitation in the region (Nesbitt *et al*., 2006). The development of these MCSs requires of intense moisture transport from the tropics to the subtropics, which is not well represented by the RCMs, Fig. 6. This figure is for the period October-March when, as will be seen in the next section, most of the MEPs take place. The observed case shows a water vapour transport from the north and two distinct areas of convergence in the east and west of LPB; in the two examples of RCM simulations, although with some differences, there is a northern transport of water vapour, but the convergence in the west area is reduced and bounded to its westernmost area near the Andes and not in the area farther east where MCS developed (Doyle *et al.* 2012).

In spite of some particularities in each model, in general they simulate correctly some of the key features of the atmospheric circulation associated with precipitation, namely the convergence of moisture in the east of SESA and the mid tropospheric circulation as indicator of cyclonic vorticity advection. It seems that the RCMs underestimation of precipitation, including that of the high percentile range, may be in part due to their lack of moisture convergence over central Argentina.

3.2.3 Correction factors

The analysis made using the control period indicates the need for some correction scheme to obtain credible estimates of future scenarios of precipitation and the related atmospheric indexes. The scheme adopted is the adjustment of the simulated distributions from models to the observed distribution (Wood, 2002). Therefore the correction factors are defined as:

$$f_i = \frac{Observed_i}{RCM's_i} \qquad (2),$$

in the case of precipitation, and

$$f_i = Observed_i - RCM's_i \quad (3)$$

for I500, DW and DE indices, where ***i*** denotes each of the percentiles.

These factors were applied to the distributions of precipitation and indices percentiles obtained from RCMs for the near future and end of century periods. More details on motivation for this correction procedure and its scheme in Saurral *et al.* (2013) in this volume. The implicit assumption in this methodology is that the factors will remain approximately constant in the projected periods.

4. RESULTS

4.1 Precipitation

4.1.1. Projection of future distributions

Figures 7, 8 and 9 show the percentile distributions of monthly precipitation for the three regions and four RCMs used in this work for the present period as compared with the observed one. This reference period was chosen as 1990/2004. In the LPB there were important trends in precipitation starting in some areas in the 1960 decade and in the 1970 in others, (Barros *et al.* 2000, Liebmann *et al.* 2004). In any case, the bulk of the change took place before 1990, while later the attained mean annual values were fluctuating without significant trends. Therefore, using a period after 1990 as reference for present conditions prevents incorrectly estimating as future changes those that already have been taken place. The limit of 2004 is because some of the data bases used are yet incomplete after that year.

Over R1, Figure 7, only the RCA model shows a persistent increase in precipitation values in the medium and high percentiles, mainly towards the end of the 21st century. For example, in the very extreme monthly precipitation of the 95 percentile, the observed value of 260 mm would increase to 359 mm in the last thirty years of the 21st century. In the case of LMDZ model, there is a trend to greater precipitations in much of the distribution toward the end of century period, but extreme monthly precipitation become more intense since the beginning of the century. RegCM3 model does not show noticeable changes in the future high percentiles but shows increases over time in the rest of distribution, especially in the 40-80 percentiles range towards the end of century, while the PROMES model does not show significant changes in none of the two future scenarios.

Over southern Brazil, in R2, RCA and LMDZ models also show increases in rainfall values for high and extreme precipitation months, being more pronounced towards the end of century. The remaining two models do not show significant changes in the distribution of monthly precipitation over time in this region.

In the south of the La Plata basin, region R3, all RCM projections are consistent in showing a clear increase in the extreme values of monthly rainfall. For the near future period there are increases only in high and the extreme rainfall values without major changes in the rest of the distribution, while by the end of the century not only the increase in the extreme precipitation values is more pronounced, but except for the PROMES model, extends to the rest of the distribution.

While RCM projections indicate the possibility of precipitation increasing with time in the three regions, this appears less ambiguous in the south of the La Plata basin and especially for extreme monthly precipitations. According to these RCM projections and being conservative, it should be ruled out the possibility that extreme precipitations would be lower than in the recent observed period.

4.1.2 Projections of the annual cycle of months with extreme precipitation

As already explained, here we define as months with extreme precipitation (MEP) those with precipitation above the mean plus one standard deviation. In SESA, the availability of moisture for heavy precipitations varies throughout the year and, is generally smaller in winter. Thus, the frequency of MEPs has a marked annual cycle in the three regions, being more frequent from October to April, figures 10, 11 and 12. According to the RCM projections, this pattern would persist throughout the 21st century and the increase in frequency would take place mostly during the warm half of the year.

Changes at monthly calendar level present a general pattern despite some differences between the four models, i.e. increase in the number of MEP in the first four months of the year, especially towards the end of the century. In this period, more than half of the January months would have extreme rainfalls according to all RCMs in the three regions, with only one exception (RCA model in R2), Figure 10, 11 and 12.

The scenarios of MEP frequency change in the spring months are highly variable between models and months, but with a similar general pattern of increasing frequency of MEP by the end of the century. Over the south of LPB, in R3, projections show a few months of extreme rainfall emerging in the cold season, which were not present in the observed period (Figure 12).

4.2 Projection of indices

In section 4.1, it was shown that according to the RCMs, there will be a general trend towards an increase in intensity and frequency of months with high and extreme precipitation in the three regions, but more unambiguously in the south of LPB. To gain some understanding of what processes may be behind these possible changes, it will be discussed the projection of the atmospheric indices associated to the occurrence of MEPs (Garavaglia *et. al.* 2012). Changes in these indices could summarize changes in circulation conditions that are related to extreme rainfalls in SESA. Since the models were unable to reproduce the observed convergence in the west of Argentina, the corresponding index, DW, is not going to be considered in these discussion.

The projections of the I500 index, Figure 13, do not show future trends towards circulations that enhance the occurrence of extreme rainfall in the region. On the contrary, there are less projected cases over 20 hPa which in a study that used a somewhat similar I500 index definition is a threshold for increasing probability of MEPs (Garavaglia *et. al.* 2012). In general, I500 tends to be slightly reduced in future scenarios of three models and considerably decreased in the case of the LMDZ model.

RCA, PROMES and LMDZ models and less clearly RegCM3 project an increase in convergence of water vapour in the region east of 60° W (DE index), Figure 14. This increase is much more evident for extreme monthly events (low percentiles) and towards end of century.

The general trend towards more precipitation in SESA in the twenty first century, especially in the case of high and extreme monthly precipitation as projected by the RCMs do not seem to respond to more cyclonic advection in the mid tropospheric circulation, but to an increase of the water vapour convergence in the lower atmosphere over the east of the subtropical SESA.

5. CONCLUDING REMARKS

During the second half of the 20th century in the LPB there was a general positive trend in precipitation starting in some areas in the 1960 decade and in the 1970 in others, (Barros *et al.* 2000, Liebmann *et al.* 2004). These trends were more evident in monthly extremes and at a spatial scale compatible with the long lasting regional floods, Doyle *et al.* (2012).

According to the four RCMs analyzed, these trends would not be reversed during the present century and will likely persist in monthly extreme precipitations as two of the four models project in northeast of Argentina and south of Brazil and all models do for the southern part of LPB, namely in region 3, Figure 1, where extended and lasting floods take place over very flat plains with small drainage. Therefore, without critical changes in other conditions, like land use or drainage works, it could be expected that present recurrence of long lasting floods will persist or even become shorter. These results bear uncertainties related to the RCMs skills, but also those depending on the realization or not of the emission scenario used to force these models, namely the SRES A1B. For the near term future, global climate would be approximately similar no matter which emission scenarios actually will take place. Therefore, emission scenarios will not affect the near term future climate and results from one emission scenario can be considered representative of any other possible one. On the contrary, since global climate by the end of the century will be critically dependable on the emission scenario, the results here presented, based on a kind of mid emission scenario, only can be seen as a qualitative approach for the sign of changes.

MEPs have a marked annual cycle in LPB, being more frequent from October to April, and according to the RCM projections this pattern would persist throughout the 21st century because their increase in frequency would take place mostly during the warm half of the year. However, in the case of the southernmost LPB region, it would appear MEPs in future scenarios during winter time, which were not observed in the reference period. This result would worse flood conditions contributing to enduring flooding because of the small evaporation in that part of the year.

The general trend towards higher extreme monthly precipitation in SESA in the twenty first century, as projected by the RCMs, seems to respond to an increase of the water vapour convergence in the lower atmosphere over the east of the subtropical SESA. Although, other factors would contribute to this increased convergence, the mere warming associated to the global climate change will contribute to it. In fact, regional warming was projected by the four RCMs here analyzed (Saurral *et al.* 2013 in this volume).

Acknowledgments: The research leading to these results has received funding from the European Community's Seventh Framework Programme (FP7/2007-2013) under Grant Agreement N° 212492

REFERENCES

Barros, V.R., Castañeda, M.E. and Doyle, M.E. 2000. Recent precipitation trends in Southern South America East of the Andes: an indication of climatic variability. *Southern Hemisphere paleo- and neoclimates. Key sites, methods, data and models.* Eds. Smolka PP and Volkheimer V. 187-206. Springer, Berlin.

Barros, V.R., Chamorro, L., Coronel, G. and Báez, J. 2004. The major discharge events in the Paraguay River; Magnitudes, source regions and climate forcings. *Journal of Hydrometeorology,* 5: 1061-1070.

Boulanger, J-P., Martinez, F. and Segura, E.C. 2007. Projection of future climate change conditions using IPCC simulations, neural networks and Bayesian statistics. Part 2: Precipitation mean state and seasonal cycle in South America. *Climate Dynamics,* 28: 255 - 271. doi 10.1007/s00382-006-0182-0.

Camilloni, I. and Barros, V. R. 2003. Extreme discharge events in the Paraná River and their climate forcing. *Journal of Hydrology,* 278: 94 - 106.

Castañeda, M.E. and Barros, V. 1994. Las tendencias de la precipitación en el Cono Sur de América al este de los Andes. *Meteorológica*, 19: 23-32.

da Rocha, R.P., Morales, C.A., Cuadra, S.V., Ambrizzi, T. 2009a. Precipitation diurnal cycle and summer climatology assessment over South America: an evaluation of regional climate model Version 3 simulations. *Journal of Geophysical Research* 114: D10108. doi: 10.1029/2008JD010212

da Rocha H.R., Manzi, A.O., Cabral, O.M., Miller S.D., and others. 2009b. Patterns of water and heat flux across a biome gradient from tropical forest to savanna in Brazil. *Journal of Geophysical Research* 114:G00B12. doi:10.1029/2007JG000640.

Domínguez, M., Gaertner, M.A., de Rosnay, P., and Losada, T. 2010. A regional climate model simulation over West Africa: parameterization tests and analysis of land surface fields". *Climate Dynamics*, 35, pp: 249-265. DOI: 10.1007/s00382-010-0769-3

Doyle, M., Saurral, R. and Barros, V. 2012. Trends in the distributions of aggregated monthly precipitation over the Plata Basin. *International Journal of Climatology,* 32: 2149-2162. DOI: 10.1002/joc.2429.

Garavaglia, C., Doyle, M. and Barros, V. 2012. Statistical Relationship Between Atmospheric Circulation and Extreme Precipitation in La Plata Basin. *Meteorological Applications*. In press

García, N. and Vargas, W. 1998. The temporal climate variability in the Rio de la Plata basin displayed by river discharges. *Climate Change*, 38: 359-379.

Genta, J.L., Perez-Iribarren, G. and Mechoso, C.R. 1998. A recent increasing trend in the streamflow of rivers in southeastern South America. *Journal of Climate,* 11: 2858-2862.

Giorgi, F. 2002. Variability and trends of sub-continental scale surface climate in the twentieth century. Part I: observations. *Climate Dynamics*, 18: 675-691

Gulizia, C., Camilloni, I. and Doyle, M. 2012. Identification of the principal patterns of summer moisture transport in South America and their representation by WCRP/CMIP3 global climate models. *Theoretical and Applied Climatology*. DOI: 10.1007/s00704-012-0729-4.

Haylock, M.R., Peterson, T.C., Alves, L.M., Ambrizzi, T., Anunciação, Y.M.T., Baez, J., Barros, V.R., Berlato, M.A., Bidegain, M., Coronel, G., Corradi, V., Garcia, V.J., Grimm, A.M., Karoly, D., Marengo, J.A., Marino, M.B., Moncunill, D.F., Nechet, D., Quintana, J., Rebello, E., Rusticucci, M., Santos, J.L., Trebejo, I. and Vincent, L.A. 2006. Trends in Total and Extreme South American Rainfall in 1960–2000 and Links with Sea Surface Temperature. *Journal of Climate*, 19: 1490-1512.

Hourdin, F., Musat, I., Bony, S., Braconnot, P., and others. 2006. The LMDZ4 general circulation model: climate performance and sensitivity to parametrized physics with emphasis on tropical convection. *Climate Dynamics*. 27:7-8, 787-813

Kalnay, E., Kanamitsu, M., Kistler, R., Collins, W., Deaven, D., Gandin, L., Iredell, M., Sha, S., White, G., Woollen, J., Zhu, Y., Chelliah, M., Ebisuzaki, W., Higgins, W., Janowiak, J., Mo, K.C., Ropelewski, C., Wang, J., Leetmaa, A., Reynolds, R., Jenne, R. and Joseph, D. 1996. The NCEP/NCAR 40-year Reanalysis Project. *Bulletin of the American Meteorological Society,* **77**: 437 – 471.

Kjellström E., Bärring L., Gollvik S., Hansson U., Jones C., and others. 2005. A 140-year simulation of European climate with the new version of the Rossby Centre regional atmospheric climate model (RCA3). *Report in Meteorology and Climatology 108,* SMHI, SE-60176 Norrköping, Sweden, 54 pp.

Latrubesse, E.M. and Brea, D. 2009. Chapter 16. Floods in Argentina. *Developments in Earth Surface Processes,* 13: 333-349.

Li, Z.-X. 1999. Ensemble atmospheric GCM simulation of climate interannual variability from 1979 to 1994. *Journal of Climate*, 12: 986–1001.

Liebmann, B., Vera, C., Carvalho, L., Camilloni, I., Barros, V., Hoerling, M. and Allured, D.A. 2004. An Observed Trend in Central South American Precipitation. *Journal of Climate,* 17: 4357-4367.

Nesbitt, S.W., Cifelli, R. and Rutledge, S.A. 2006. Storm morphology and rainfall characteristics of TRMM precipitation features. *Monthly Weather Review,* 134: 2702-2721.

Pal, J. S., and Coauthors. 2007. Regional climate modeling for the developing world: The ICTP RegCM3 and RegCNET. *Bulletin of the American Meteorological Society*, 88, 1395–1409.

Penalba, O.C. and Robledo, F.A. 2009. Spatial and temporal variability of the frequency of extreme daily rainfall regime in the La Plata Basin during the 20th century. *Climatic Change*, 98: 531-550.

Re, M. and Barros, V.R. 2009. Extreme rainfalls in SE South America. *Climatic Change,* 96: 119-136.

Salio, P.V., Nicolini, M. and Zipser, E.J. 2007. Mesoscale convective systems over southeastern South America and their relationship with the South American Low-Level Jet. *Monthly Weather Review,* 135: 1290-1309.

Samuelsson, P., Gollvik, S. and Ullerstig, A. 2006. The land-surface scheme of the Rossby Centre regional atmospheric climate model (RCA3). *Report in Meteorology 122*. SMHI, SE-60176 Norrköping, Sweden, 25 pp.

Sánchez, E., Gaertner, M. A., Gallardo, C., Padorno, E., Arribas, A. and co-authors. 2007a. Impacts of a change in vegetation description on simulated European summer present-day and future climates. *Climate Dynamics*. 29*,* 319–332.

Saurral, R. 2010. The hydrologic cycle of the La Plata Basin in the WCRP-CMIP3 multi-model dataset. *Journal of Hydrometeorology,* 5: 1083-1102.

Saurral, R., Montroull, N. and Camilloni, I. 2013. Development of statistically unbiased 21st Century hydrology scenarios over La Plata Basin. Submitted to *International Journal on River Basin Management.* Special Issue on La Plata Basin, this volume.

Seth, A., Rauscher, S.A., Carmago, S.J., Quian, J-H, Pal, J.S. 2007. RegCM3 regional climatologies for South America using reanalysis and ECHAM global model driving fields. *Climate Dynamics*, 28, pp. 461–480.

Solman, S.A., Le Treut, H. 2006. Climate change in terms of modes of atmospheric variability and circulation regimes over southern South America. *Climate Dynamics*, 26: 835-854.

Vera, C.S. and Silvestri, G. 2009. Precipitation interannual variability in South America from the WCRP-CMIP3 multi-model dataset. *Climate Dynamics*, 32: 1003-1014.

Wood, A. W., Maurer, E.P., Kumar, A., and Lettenmaier, D.P. 2002: Long-range experimental hydrologic forecasting for the eastern United States. *J. Geophys. Res.*, 107, 4429, doi:10.1029/ 2001JD000659.

FIGURE CAPTIONS

Figure 1: Regions and precipitation stations.

Figure 2: Percentile distribution of monthly precipitation averaged over regions a) R1, b) R2 and c) R3 for the control period 1981/1990. Black for the observed values and simulated by models RC (green), RegCM3 (violet), LMDZ (blue) and PROMES (orange).

Figure 3: Percentile distribution of the I500 index. According to the definition of the index, positive (negative) values indicate prevailing cyclonic (anticyclonic) advection over SESA. Colours as in Figure 2.

Figure 4: Percentile distribution of the DE index. According to the definition of the index, positive (negative) values indicate prevailing divergence (convergence) of water vapour in the low levels of the atmosphere in SESA. Colours as in Figure 2.

Figure 5: As in Figure 4 but for the DW index.

Figure 6: Mean water transport (arrows) integrated between 1000 and 700 hPa (mm m s^{-1}) and its divergence in contours (10^{-5} mm s^{-1}) for the period October-March. a) Observed, b) RCA model and c) RegCM3 model. The boxes indicate the areas where DW and DE indexes are calculated

Figure 7: Percentile distribution of monthly precipitation of RCM models averaged over region R1, a) RCA, b) PROMES, c) RegCM3, d) LMDZ for the near future (blue) and for the end of the century (green). In black the observed distribution for the 1990-2004 period.

Figure 8: As in Figure 7, but for region R2.

Figure 9: As in Figure 7, but for region R3.

Figure 10: Annual cycle of the frequency of MEPs for region R1. Observed values 1990-2004 in black. Model projections for the near future in panel a) and for the end of the century in panel b), RCA in green, RegCM3 in violet, LMDZ in light blue and PROMES in orange.

Figure 11: As in Figure 10, but for region R2.

Figure 12: As in Figure 10, but for region R3.

Figure 13: Percentile distribution of projected I500 index. a) RCA, b) PROMES, c) RegCM3, d) LMDZ for the near future (blue) and for the end of the century (green). In black the observed distribution for the 1990-2004 period.

Figure 14: Percentile distribution of projected DE index. a) RCA, b) PROMES, c) RegCM3, d) LMDZ for the near future (blue) and for the end of the century (green). In black the observed distribution for the 1990-2004 period.

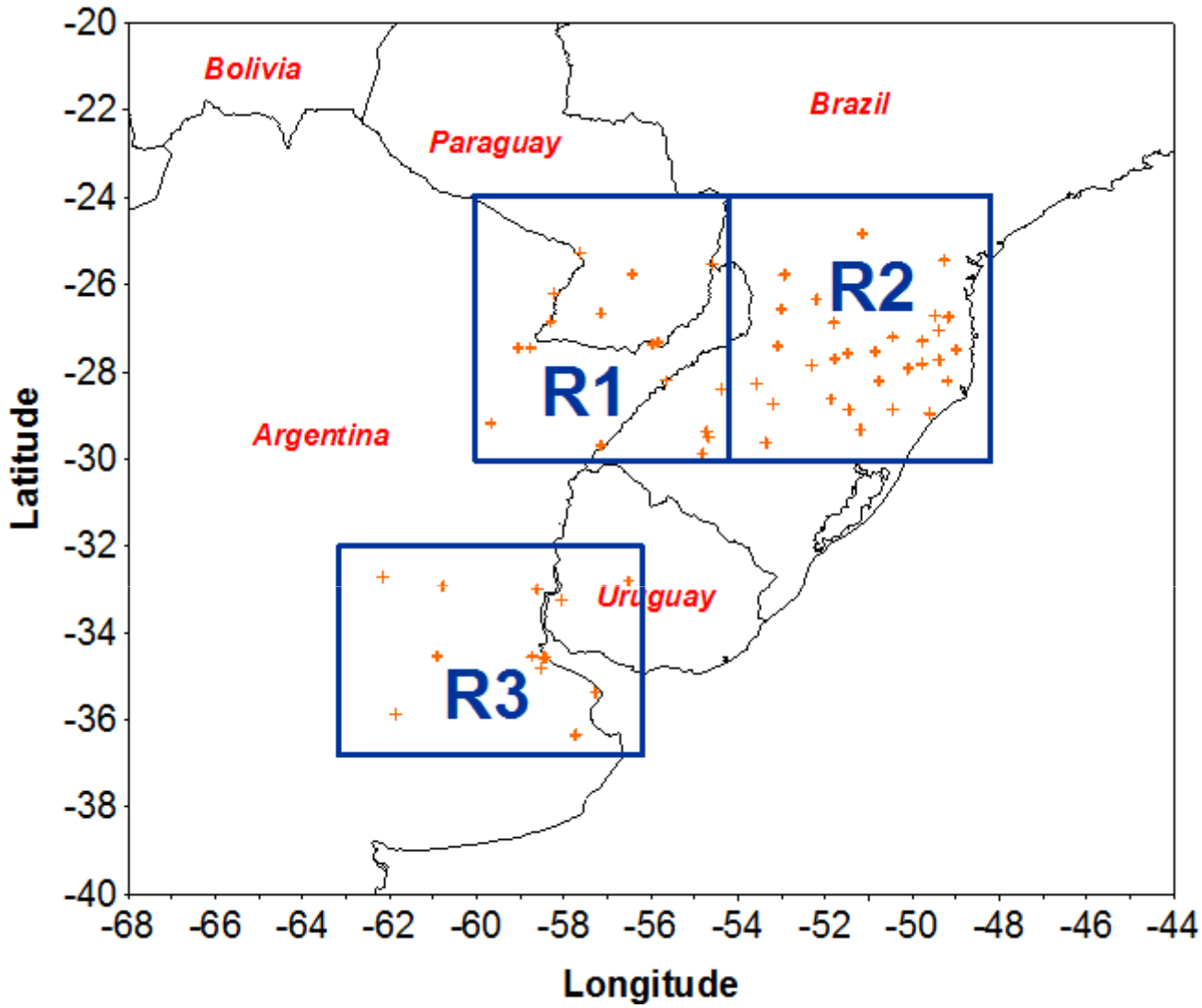

Figure 1: Regions and precipitation stations.

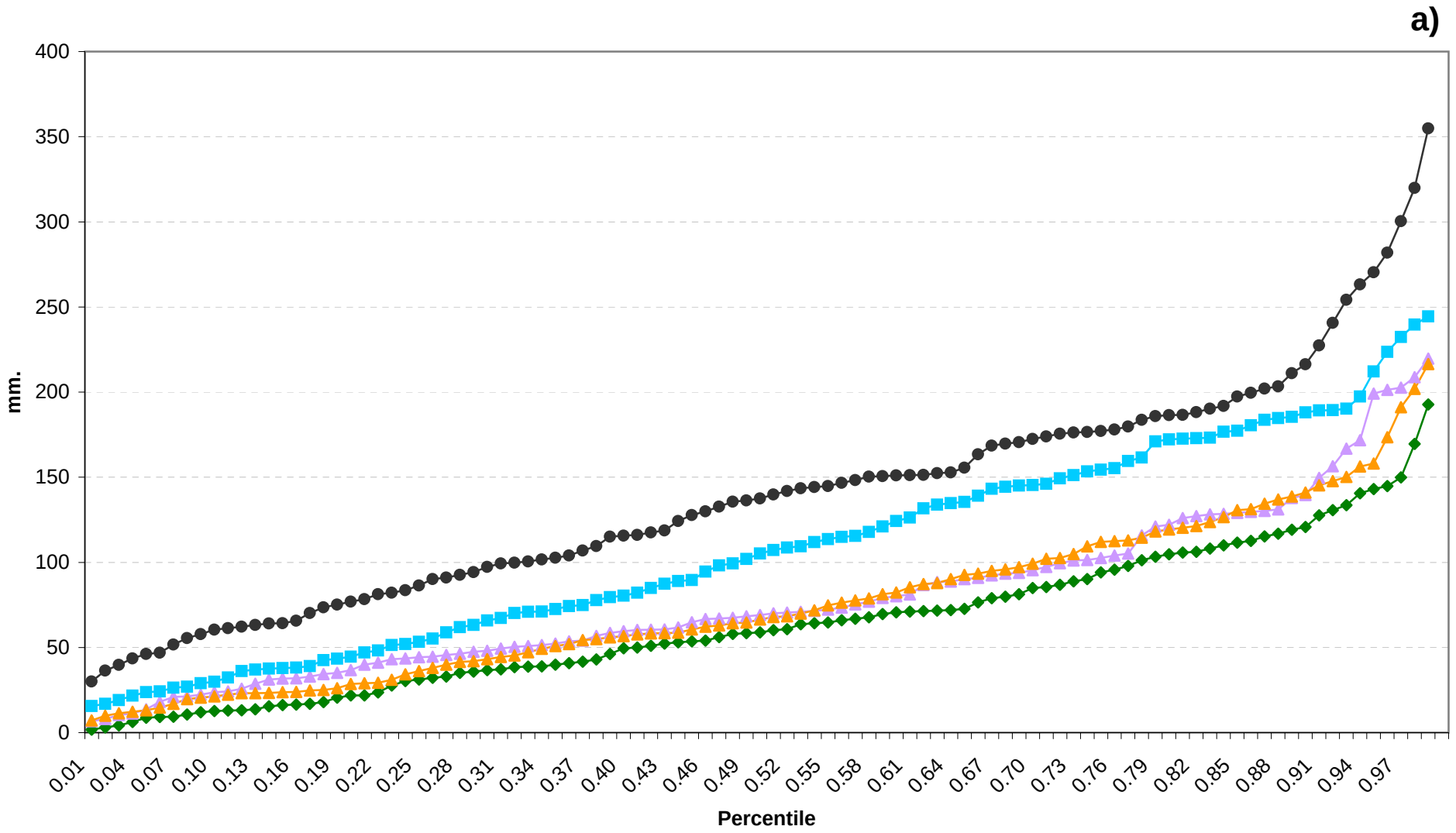
a)
400
350
300
250
200
150
100
50
0
mm.
0.01
0.04
0.07
0.10
0.13
0.16
0.19
0.22
0.25
0.28
0.31
0.34
0.37
0.40
0.43
0.46
0.49
0.52
0.55
0.58
0.61
0.64
0.67
0.70
0.73
0.76
0.79
0.82
0.85
0.88
0.91
0.94
0.97
Percentile

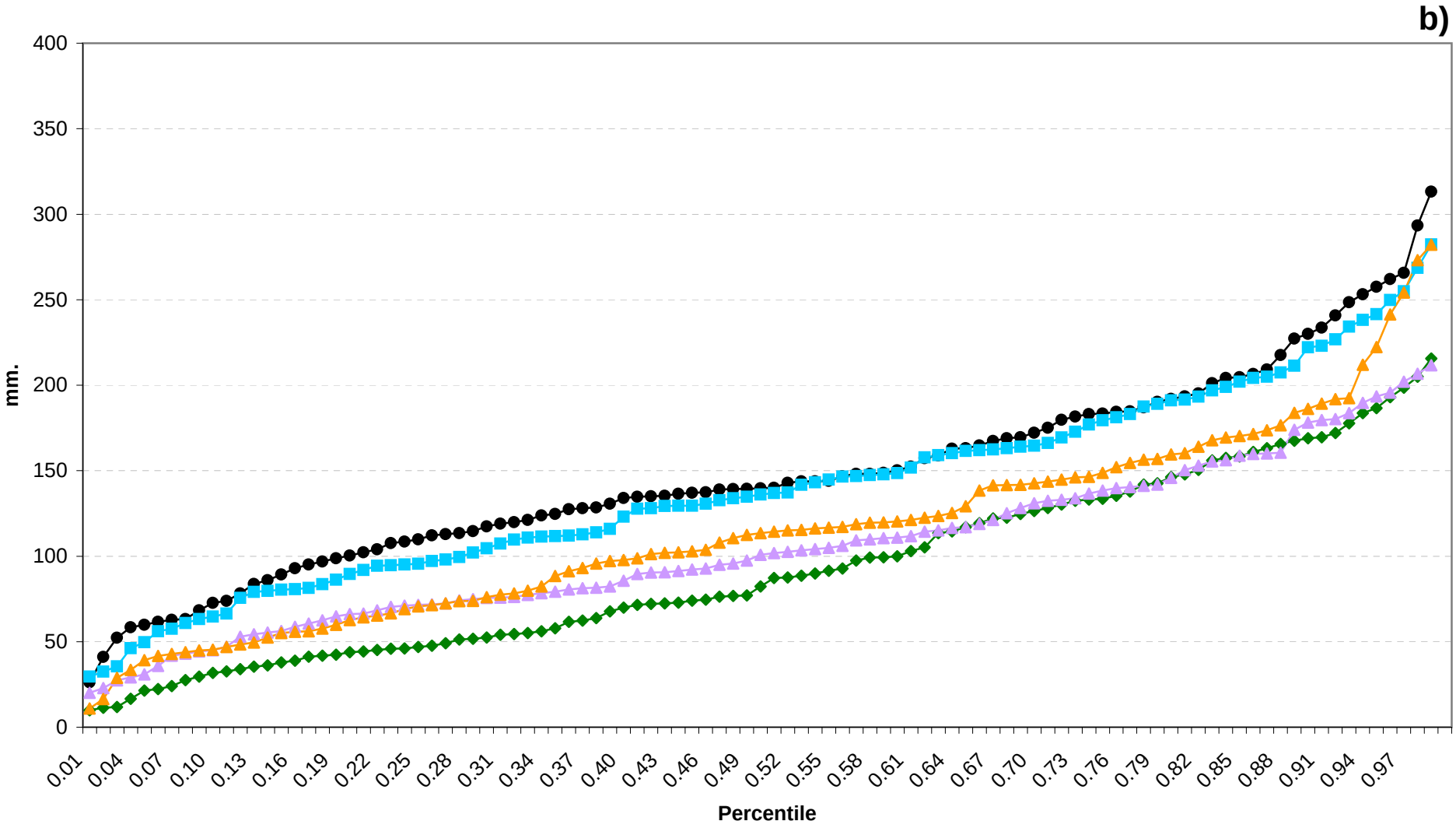
b)
400
350
300
250
200
150
100
50
0
mm.
0.01
0.04
0.07
0.10
0.13
0.16
0.19
0.22
0.25
0.28
0.31
0.34
0.37
0.40
0.43
0.46
0.49
0.52
0.55
0.58
0.61
0.64
0.67
0.70
0.73
0.76
0.79
0.82
0.85
0.88
0.91
0.94
0.97
Percentile

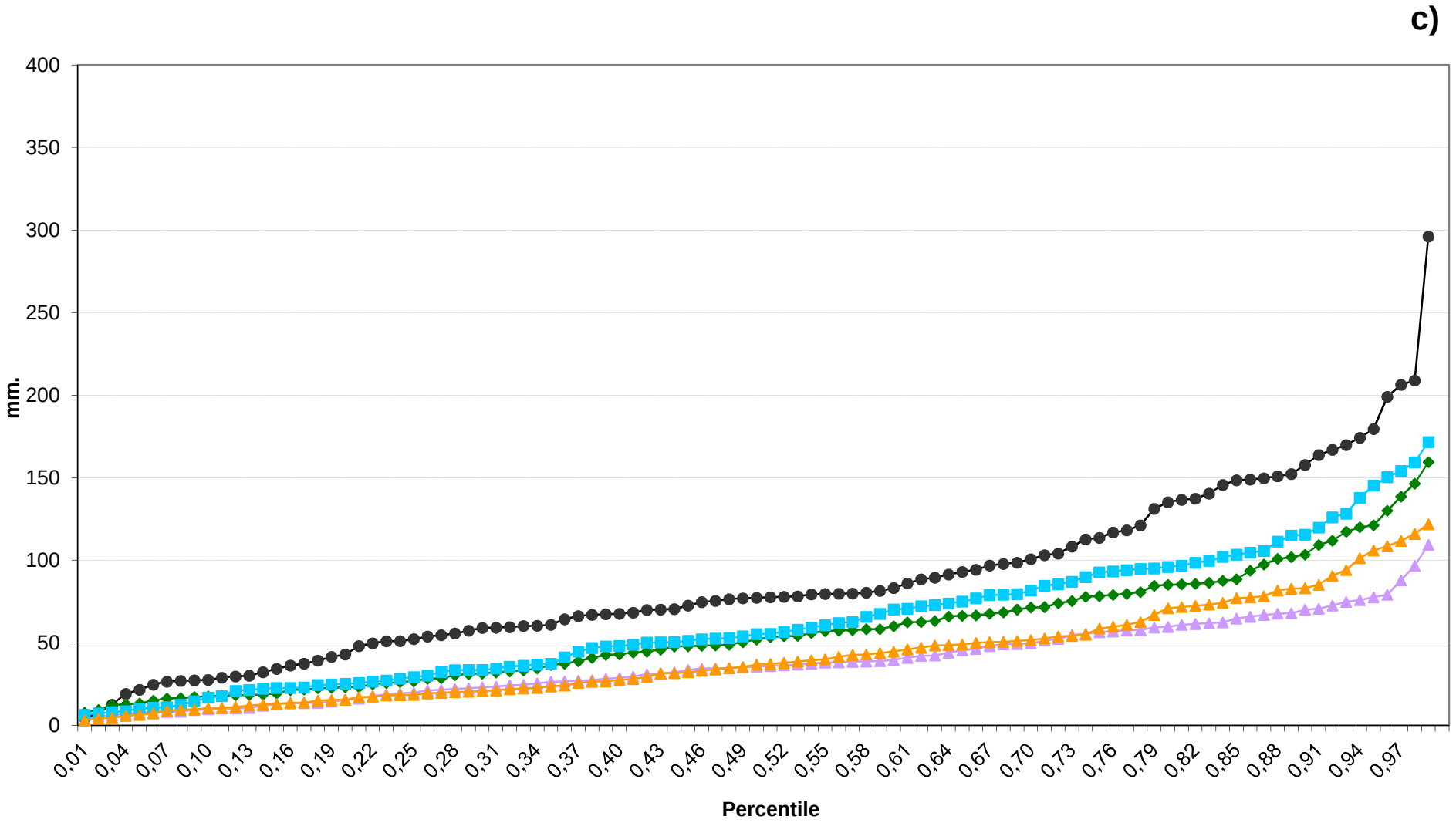

Figure 2: Percentile distribution of monthly precipitation averaged over regions a) R1, b) R2 and c) R3 for the control period 1981/1990. Black for the observed values and simulated by models RC (green), RegCM3 (violet), LMDZ (blue) and PROMES (orange).

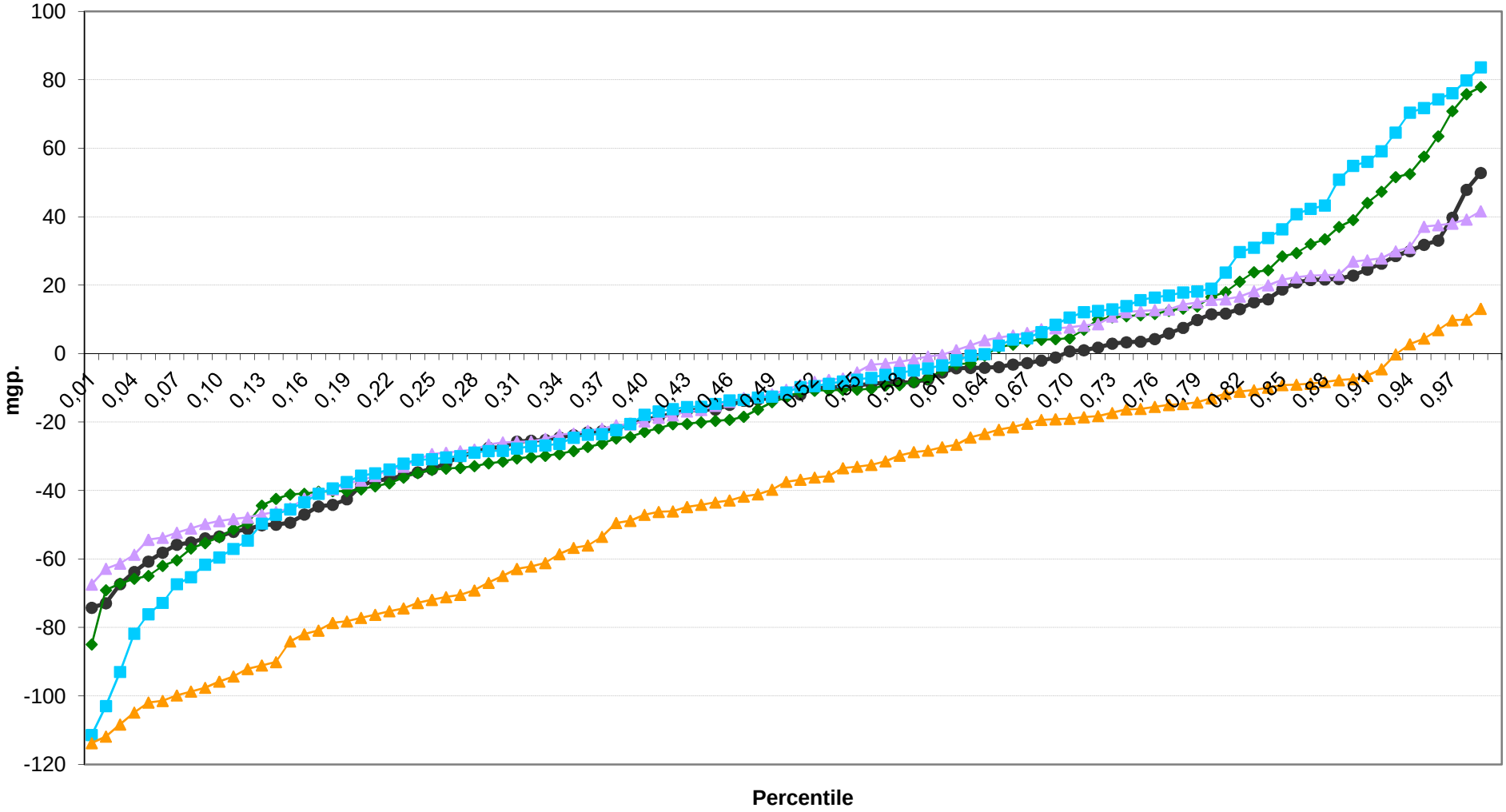

Figure 3: Percentile distribution of the I500 index. According to the definition of the index, positive (negative) values indicate prevailing cyclonic (anticyclonic) advection over SESA. Colours as in Figure 2.

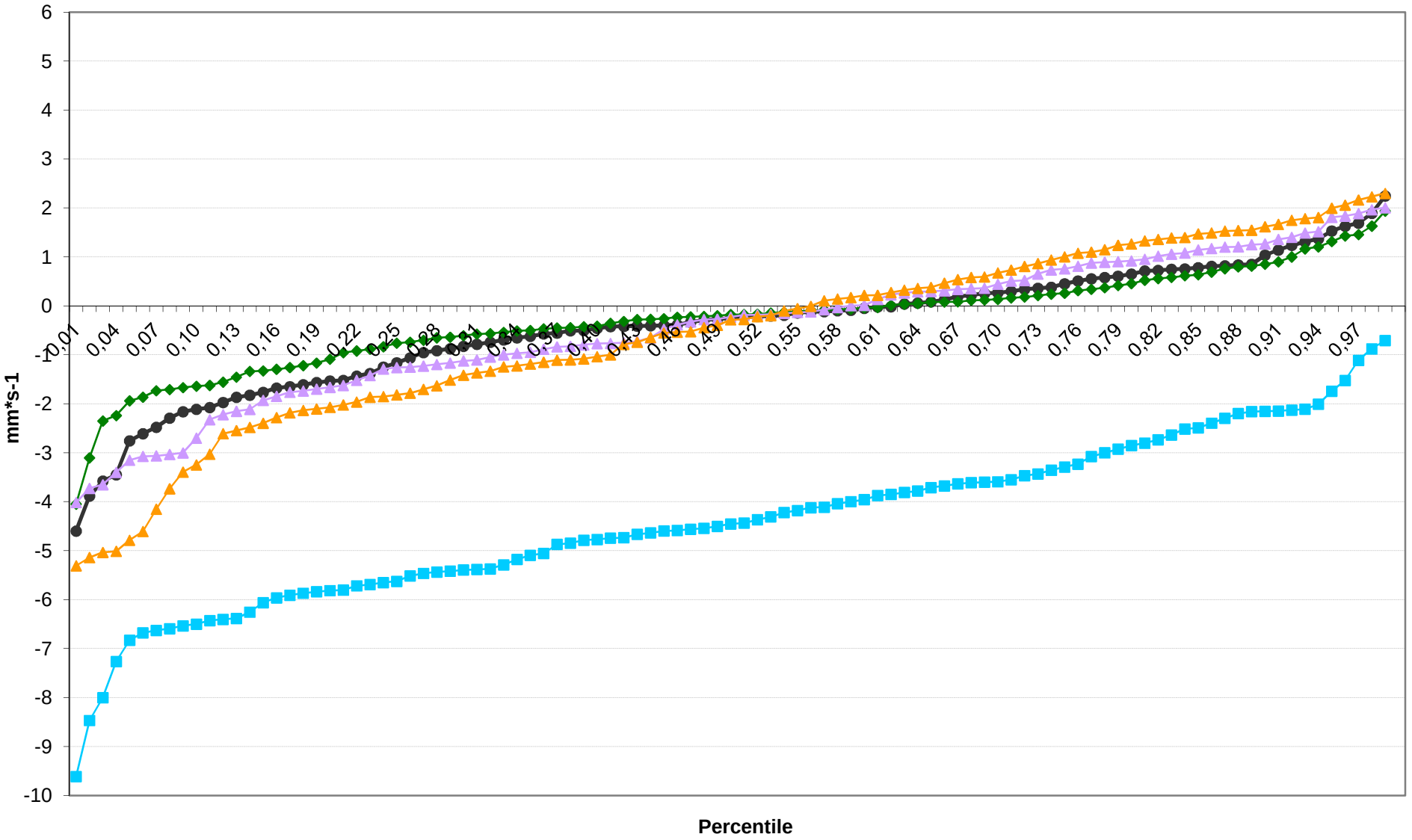

Figure 4: Percentile distribution of the DE index. According to the definition of the index, positive(negative) values indicate prevailing divergence (convergence) of water vapour in the low levels of the atmosphere in SESA. Colours as in Figure 2.

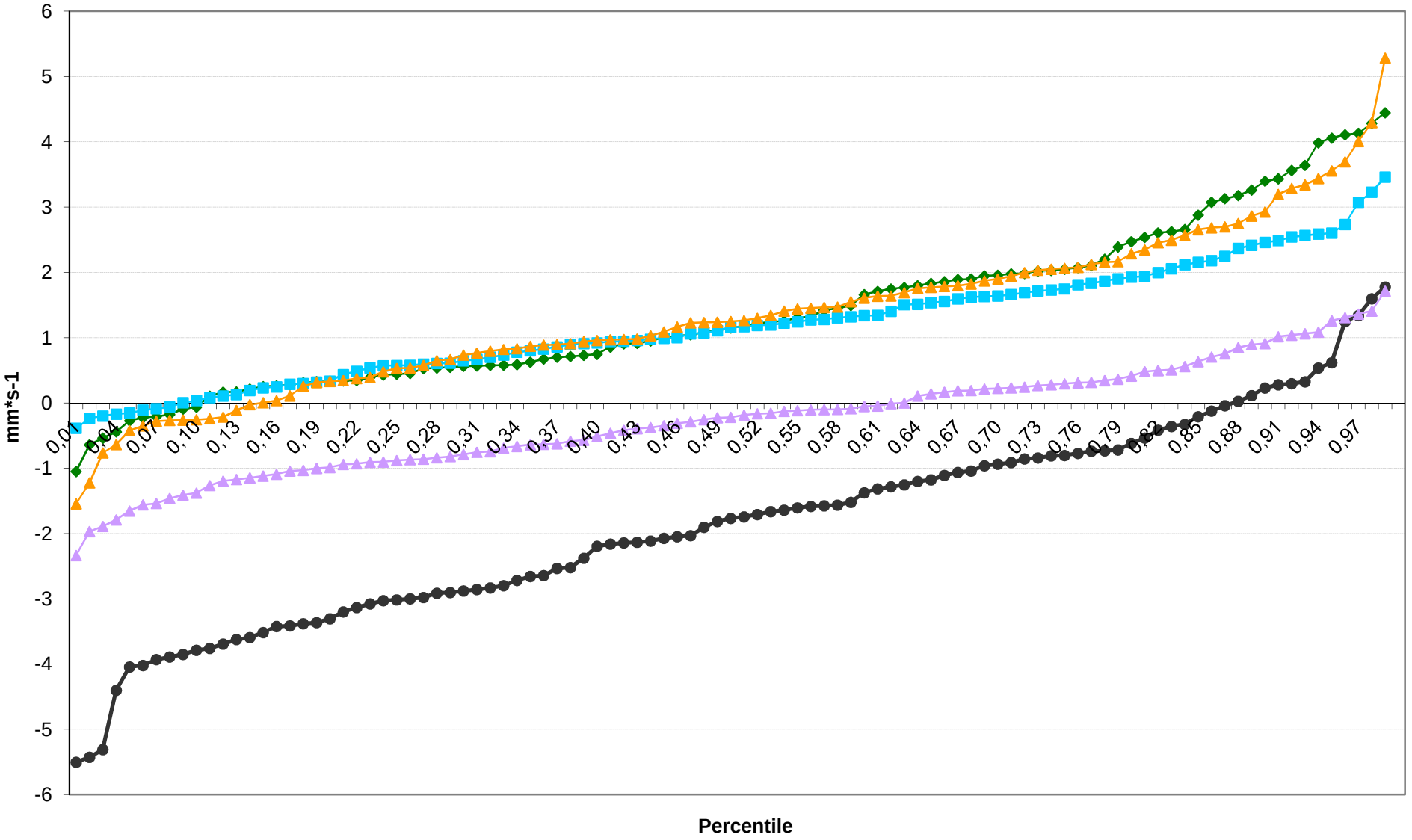

Figure 5: As in Figure 4 but for the DW index.

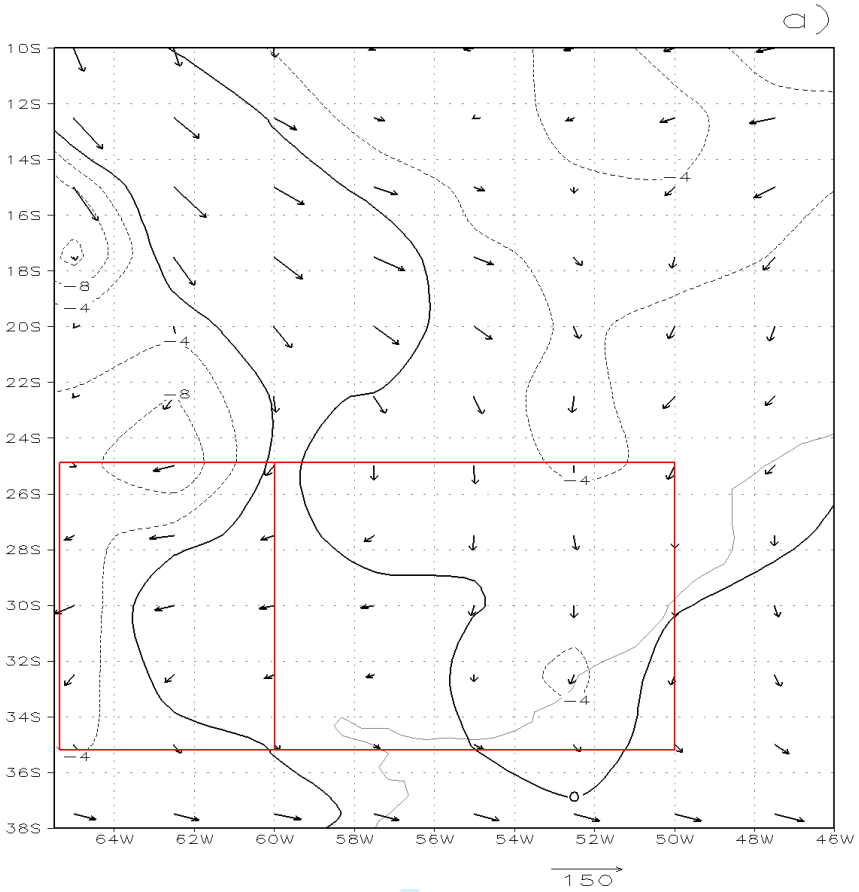

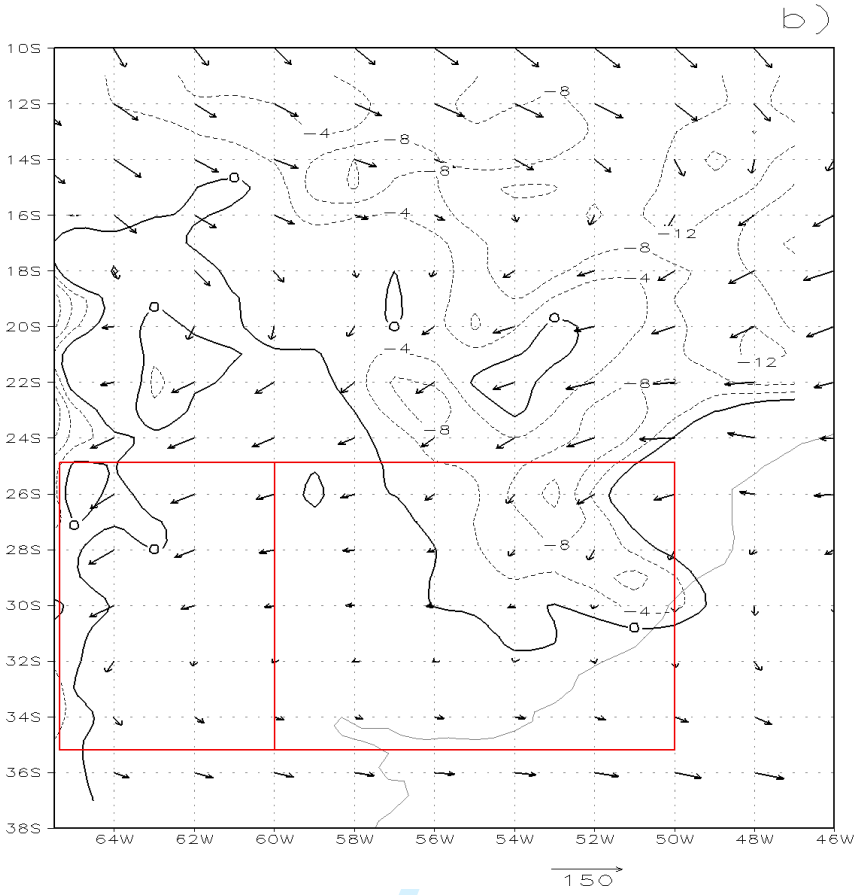
b)
10S
12S
14S
16S
18S
20S
22S
24S
26S
28S
30S
32S
34S
36S
38S
64W
62W
60W
58W
56W
54W
52W
50W
48W
46W
150

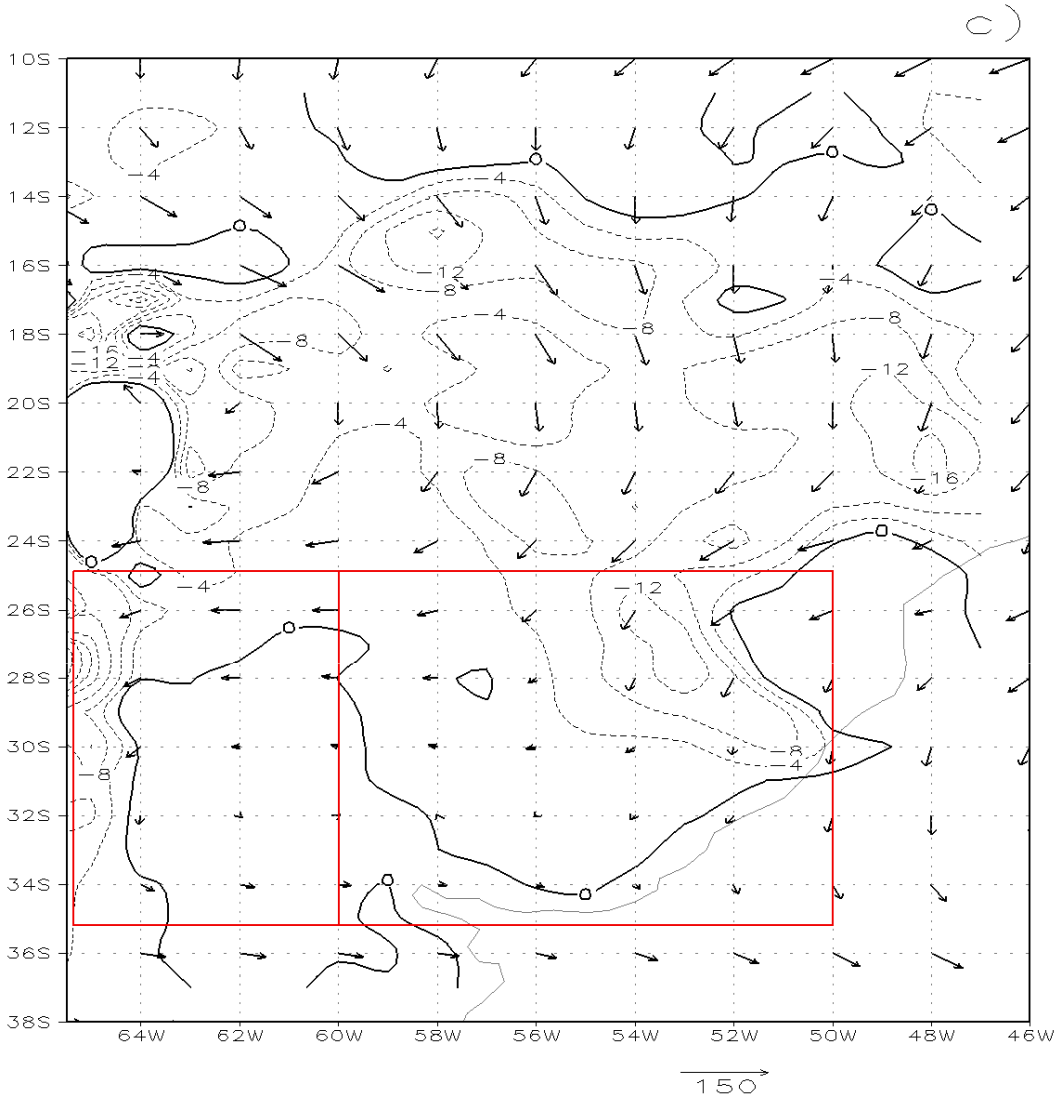

Figure 6: Mean water transport (arrows) integrated between 1000 and 700 hPa (mm m s-1) and its divergence in contours (10-5 mm s-1) for the period October-March. a) Observed, b) RCA model and c) RegCM3 model. The boxes indicate the areas where DW and DE indexes are calculated

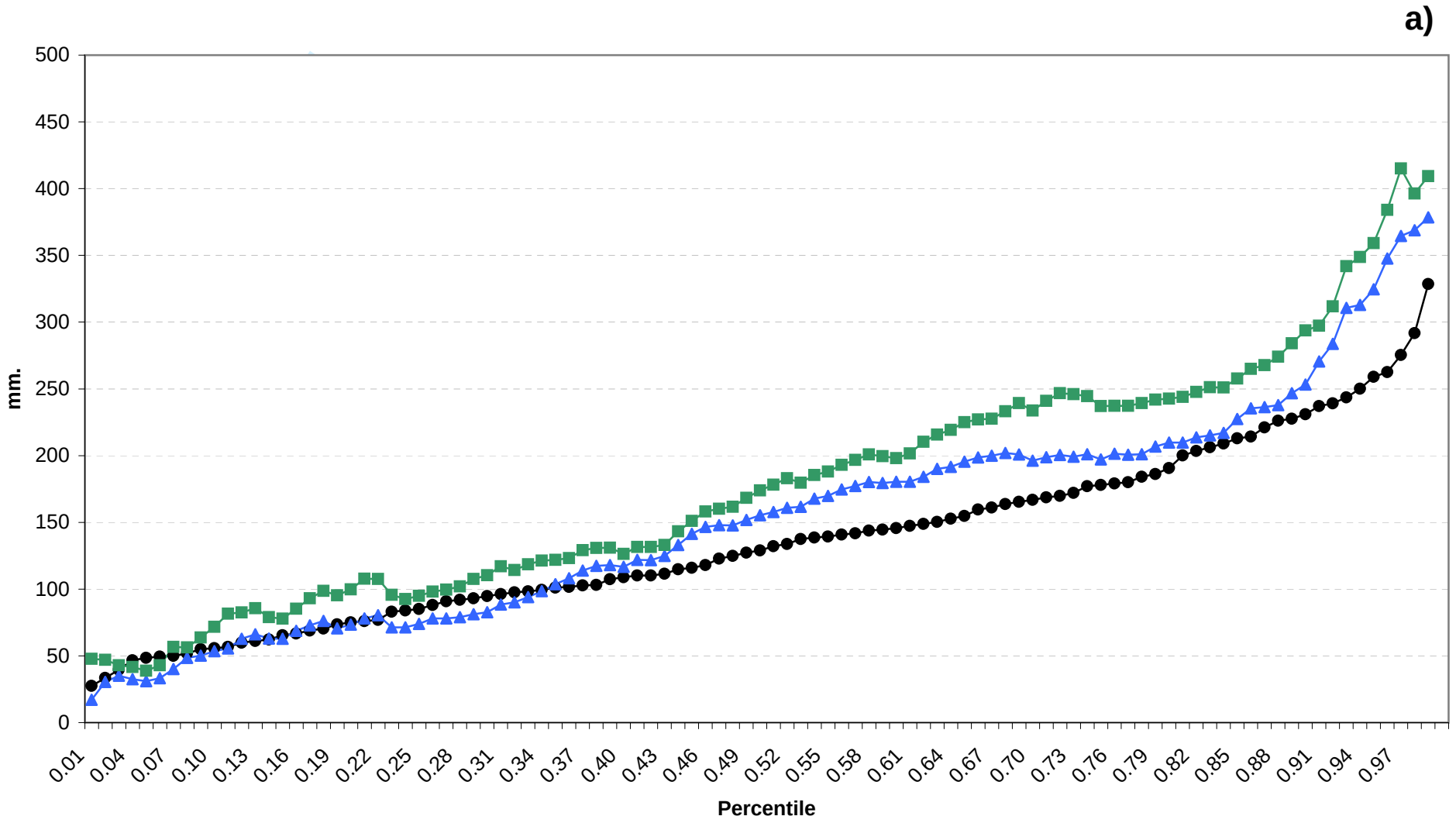
a)
500
450
400
350
300
250
200
150
100
50
0
mm.
0.01
0.04
0.07
0.10
0.13
0.16
0.19
0.22
0.25
0.28
0.31
0.34
0.37
0.40
0.43
0.46
0.49
0.52
0.55
0.58
0.61
0.64
0.67
0.70
0.73
0.76
0.79
0.82
0.85
0.88
0.91
0.94
0.97
Percentile

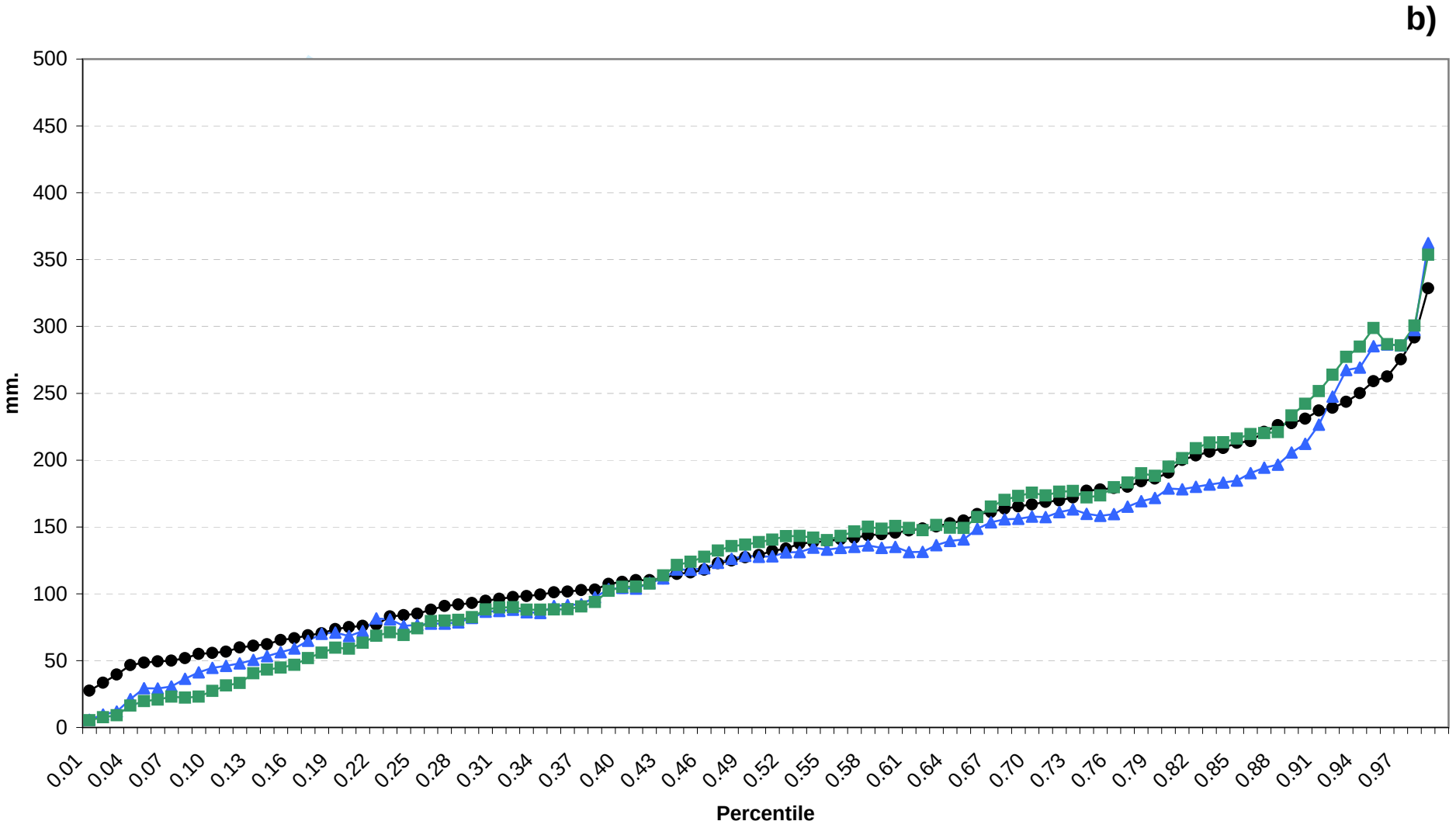
b)
500
450
400
350
300
250
200
150
100
50
0
mm.
0.01
0.04
0.07
0.10
0.13
0.16
0.19
0.22
0.25
0.28
0.31
0.34
0.37
0.40
0.43
0.46
0.49
0.52
0.55
0.58
0.61
0.64
0.67
0.70
0.73
0.76
0.79
0.82
0.85
0.88
0.91
0.94
0.97
Percentile

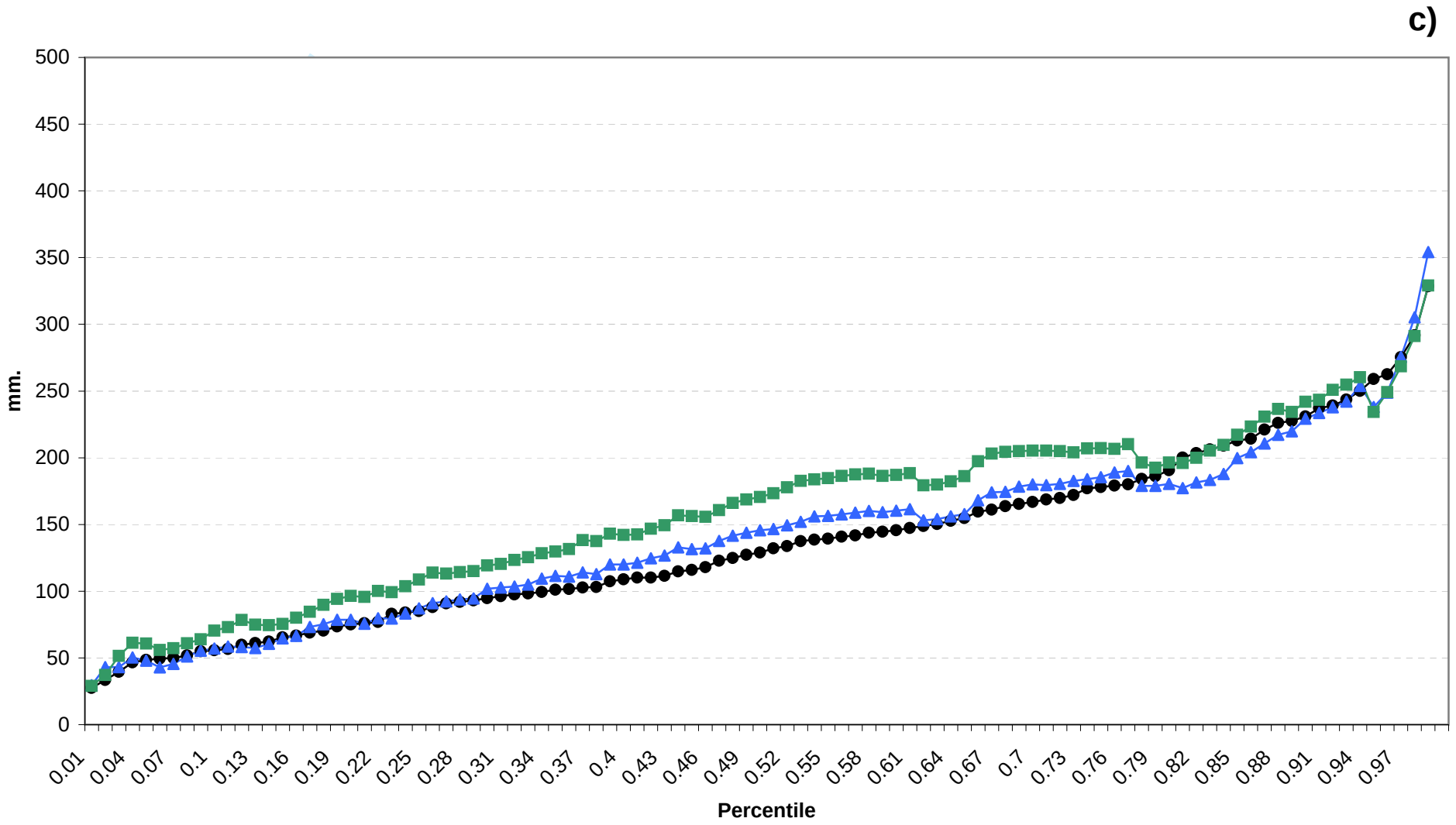
c)
500
450
400
350
300
250
200
150
100
50
0
mm.
0.01
0.04
0.07
0.1
0.13
0.16
0.19
0.22
0.25
0.28
0.31
0.34
0.37
0.4
0.43
0.46
0.49
0.52
0.55
0.58
0.61
0.64
0.67
0.7
0.73
0.76
0.79
0.82
0.85
0.88
0.91
0.94
0.97
Percentile

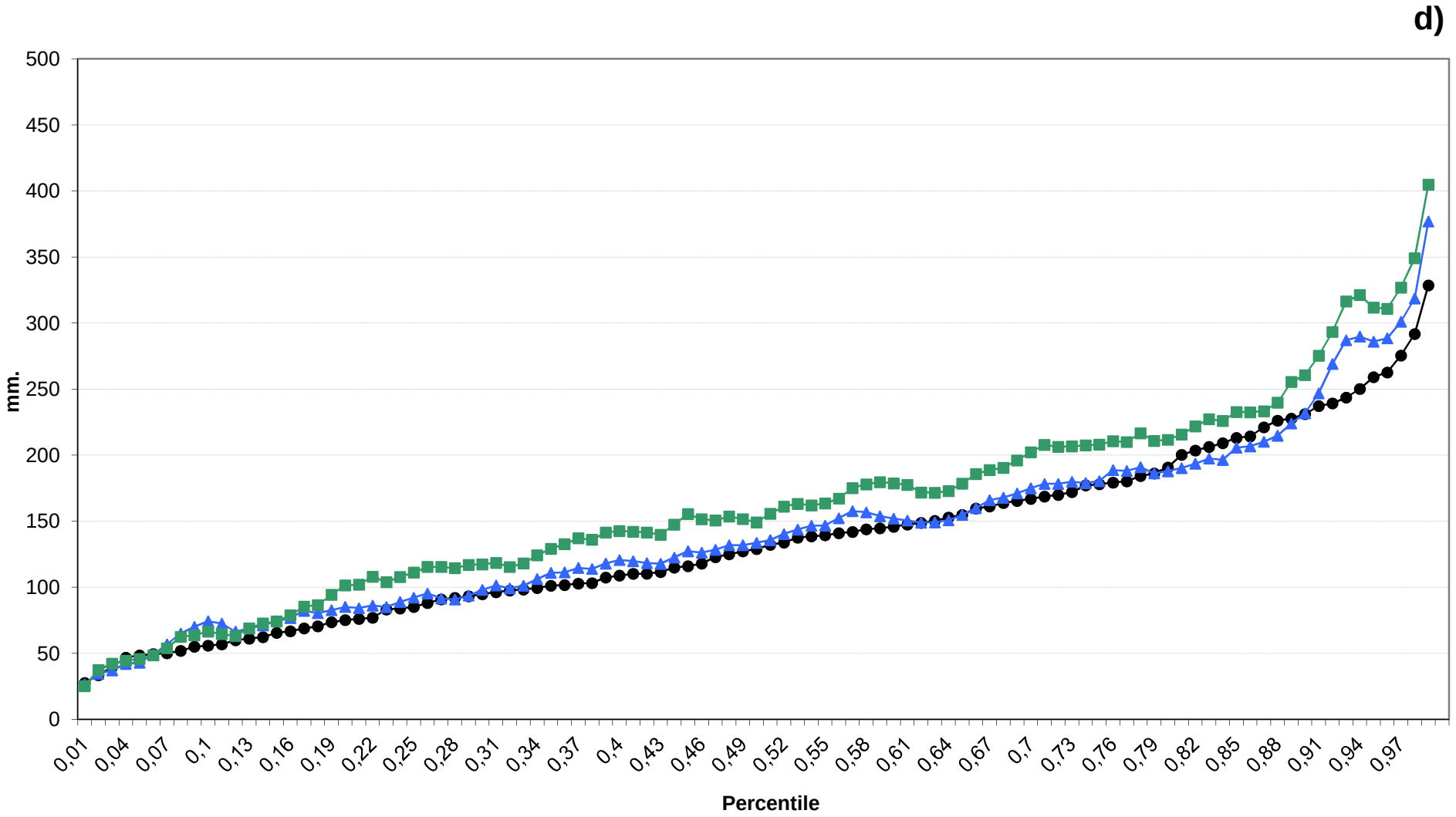

Figure 7: Percentile distribution of monthly precipitation of RCM models averaged over region R1, a) RCA, b) PROMES, c) RegCM3, d) LMDZ for the near future (blue) and for the end of the century (green). In black the observed distribution for the 1990-2004 period.

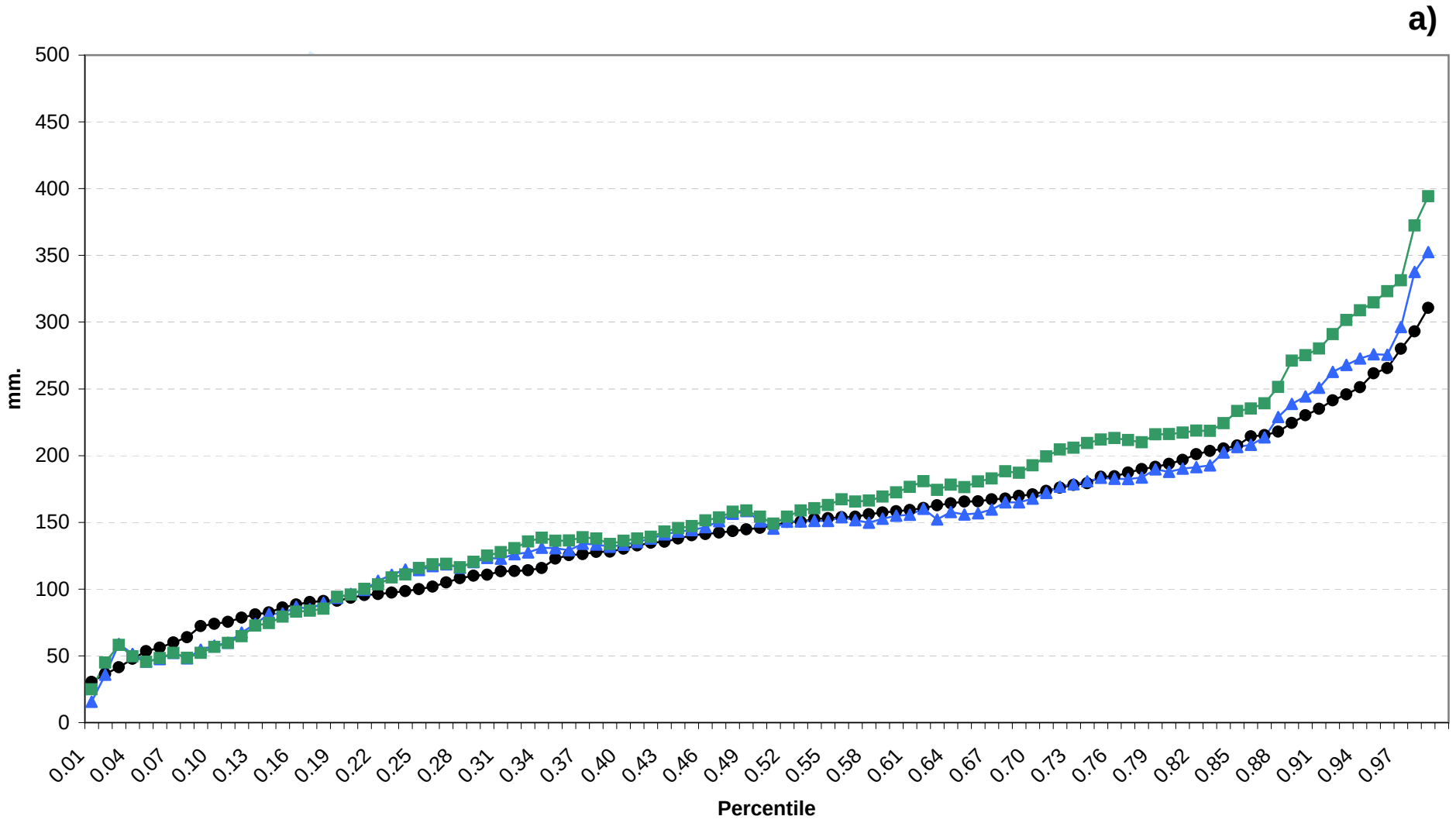
a)
500
450
400
350
300
250
200
150
100
50
0
mm.
0.01
0.04
0.07
0.10
0.13
0.16
0.19
0.22
0.25
0.28
0.31
0.34
0.37
0.40
0.43
0.46
0.49
0.52
0.55
0.58
0.61
0.64
0.67
0.70
0.73
0.76
0.79
0.82
0.85
0.88
0.91
0.94
0.97
Percentile

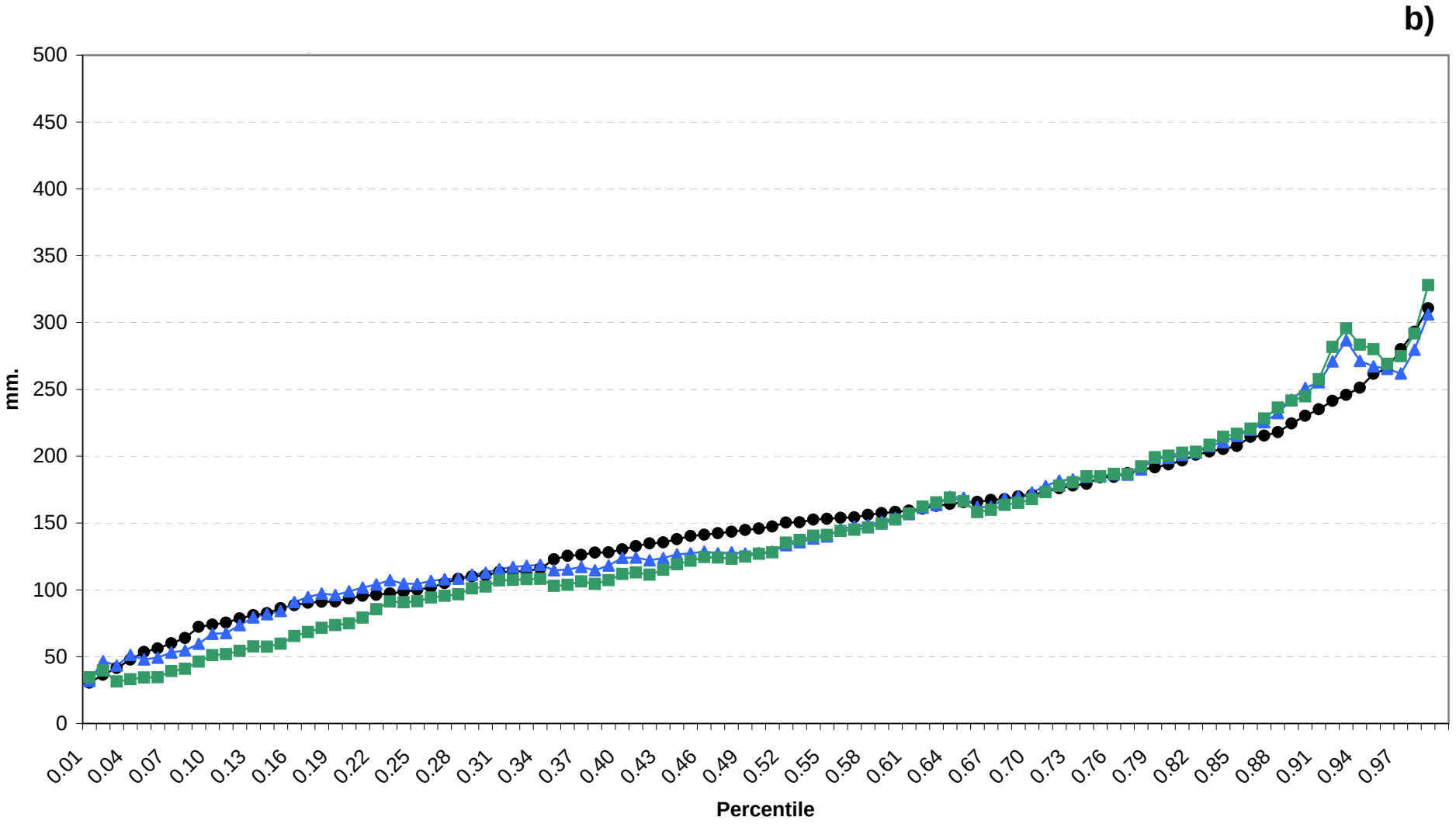
b)
500
450
400
350
300
250
200
150
100
50
0
mm.
0.01
0.04
0.07
0.10
0.13
0.16
0.19
0.22
0.25
0.28
0.31
0.34
0.37
0.40
0.43
0.46
0.49
0.52
0.55
0.58
0.61
0.64
0.67
0.70
0.73
0.76
0.79
0.82
0.85
0.88
0.91
0.94
0.97
Percentile

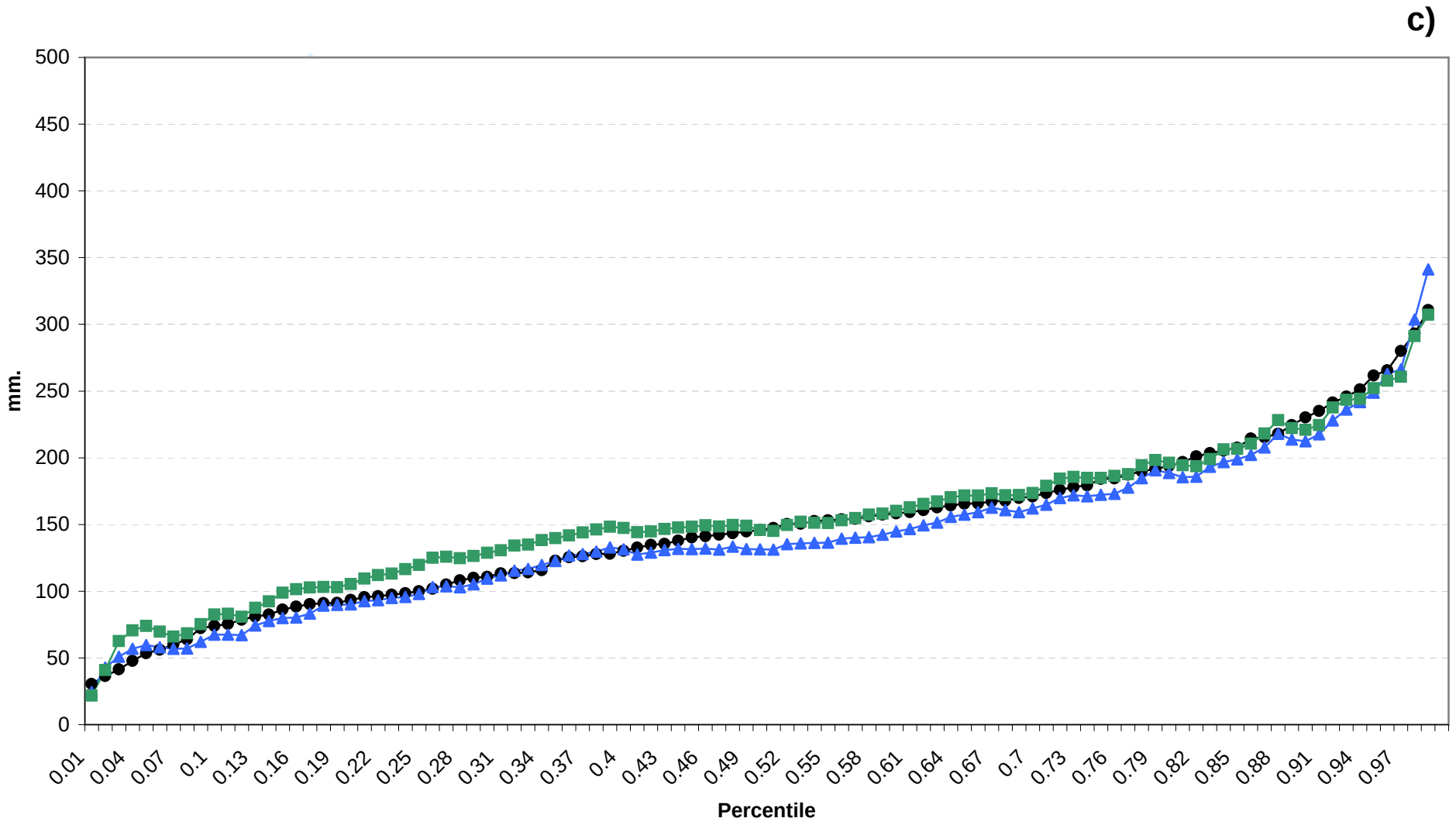
c)
500
450
400
350
300
250
200
150
100
50
0
mm.
0.01
0.04
0.07
0.1
0.13
0.16
0.19
0.22
0.25
0.28
0.31
0.34
0.37
0.4
0.43
0.46
0.49
0.52
0.55
0.58
0.61
0.64
0.67
0.7
0.73
0.76
0.79
0.82
0.85
0.88
0.91
0.94
0.97
Percentile

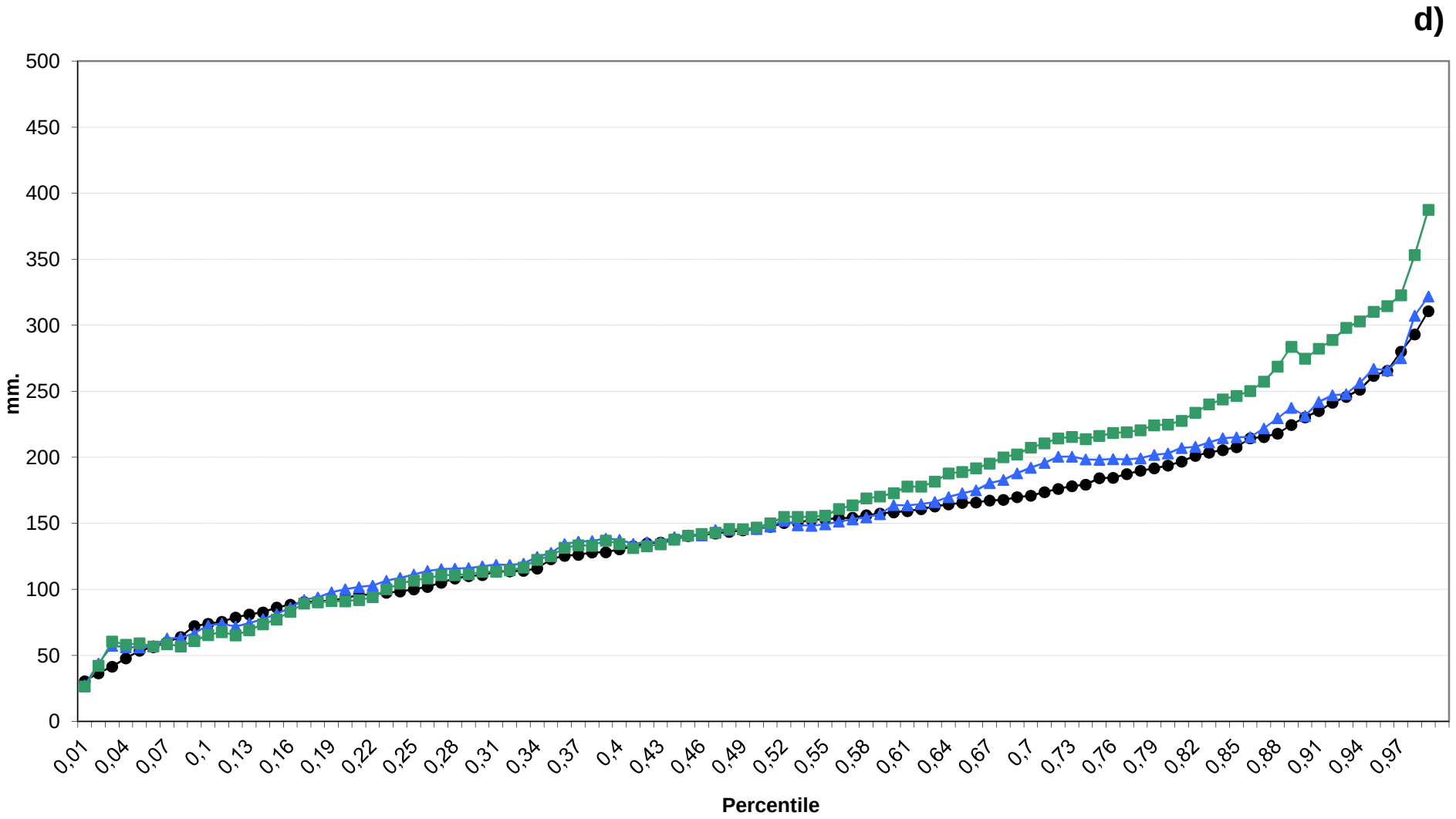

Figure 8: As in Figure 7, but for region R2.

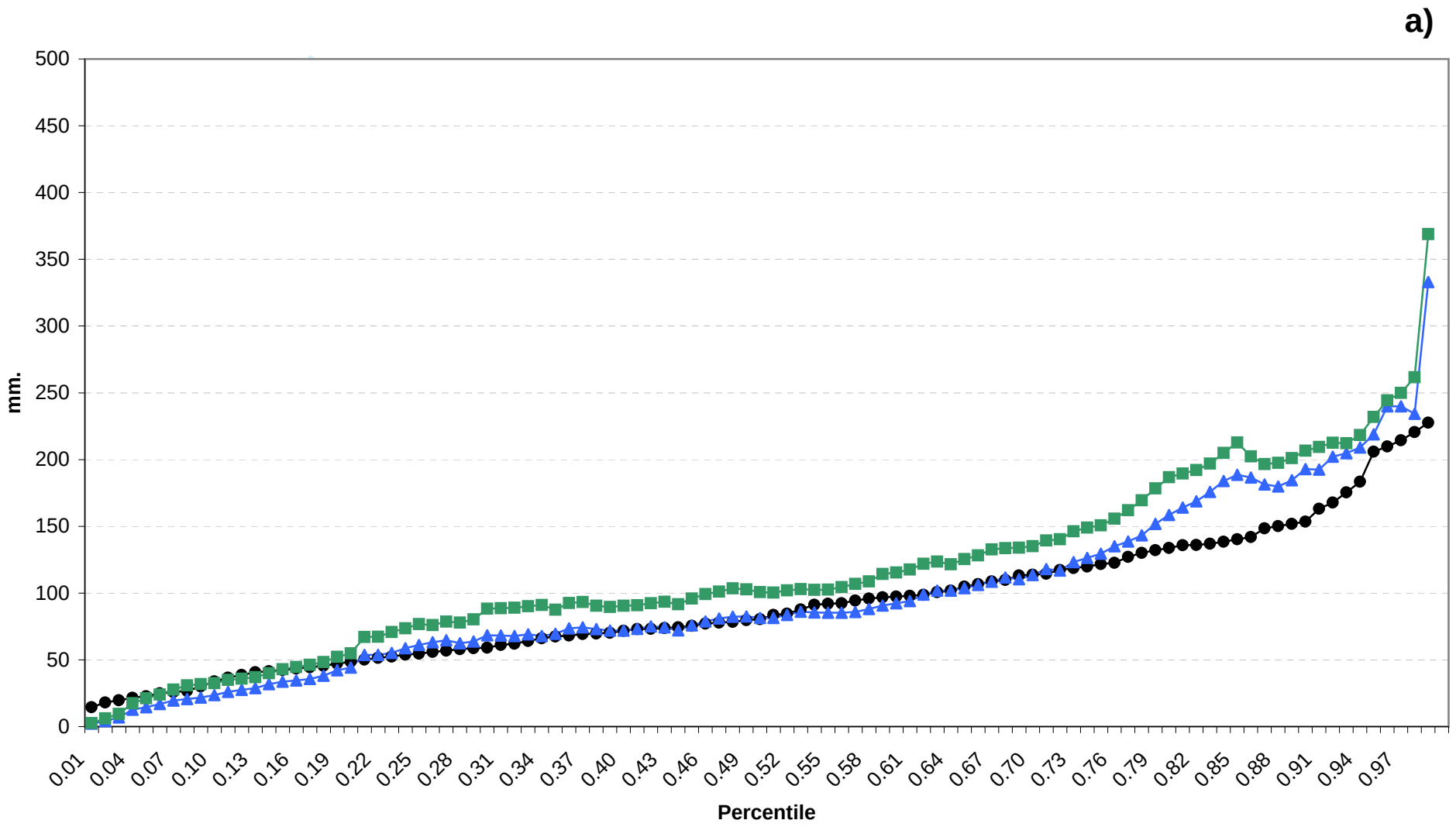
a)
500
450
400
350
300
250
200
150
100
50
0
mm.
0.01
0.04
0.07
0.10
0.13
0.16
0.19
0.22
0.25
0.28
0.31
0.34
0.37
0.40
0.43
0.46
0.49
0.52
0.55
0.58
0.61
0.64
0.67
0.70
0.73
0.76
0.79
0.82
0.85
0.88
0.91
0.94
0.97
Percentile

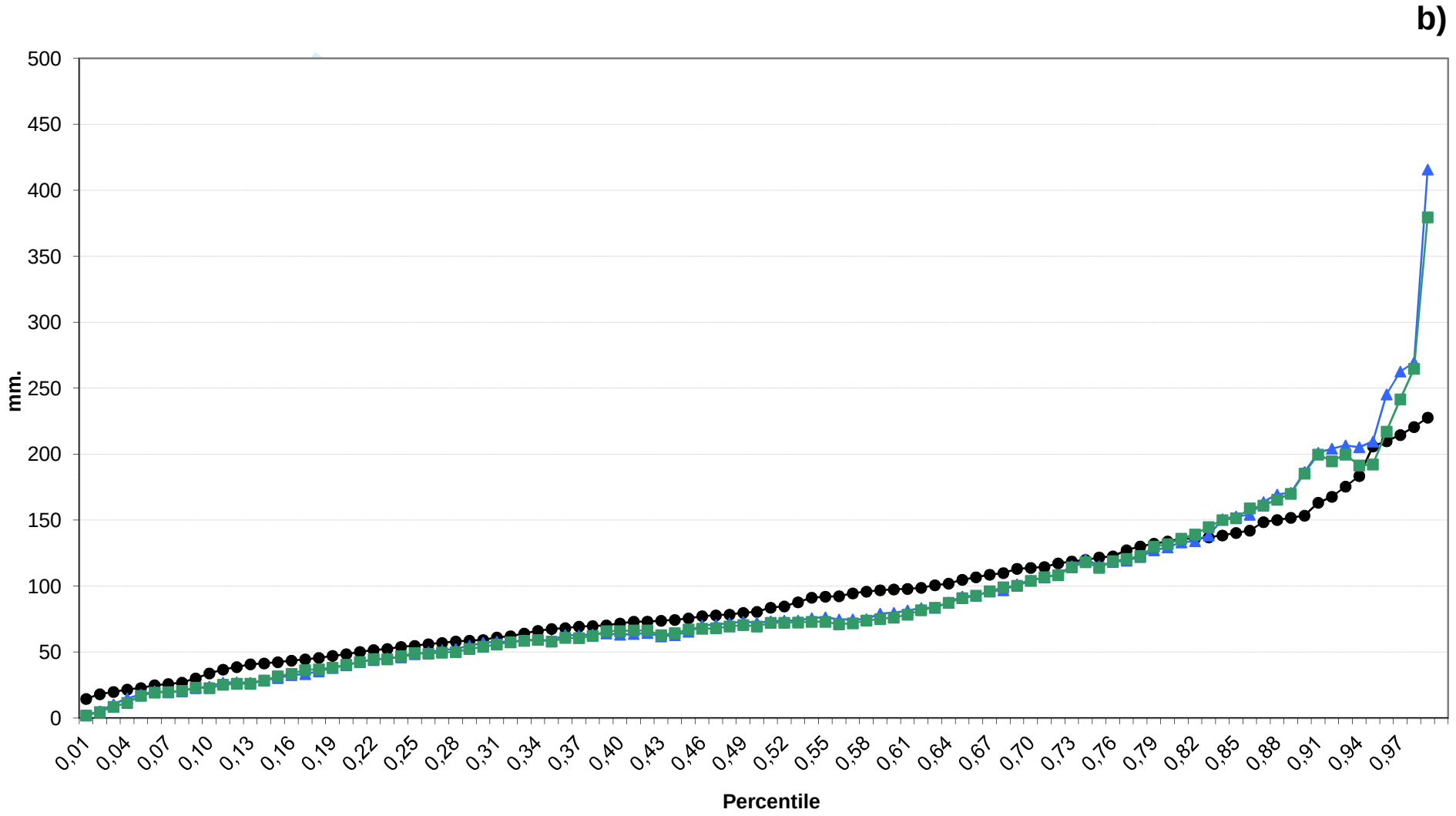
b)
500
450
400
350
300
250
200
150
100
50
0
mm.
0,01
0,04
0,07
0,10
0,13
0,16
0,19
0,22
0,25
0,28
0,31
0,34
0,37
0,40
0,43
0,46
0,49
0,52
0,55
0,58
0,61
0,64
0,67
0,70
0,73
0,76
0,79
0,82
0,85
0,88
0,91
0,94
0,97
Percentile

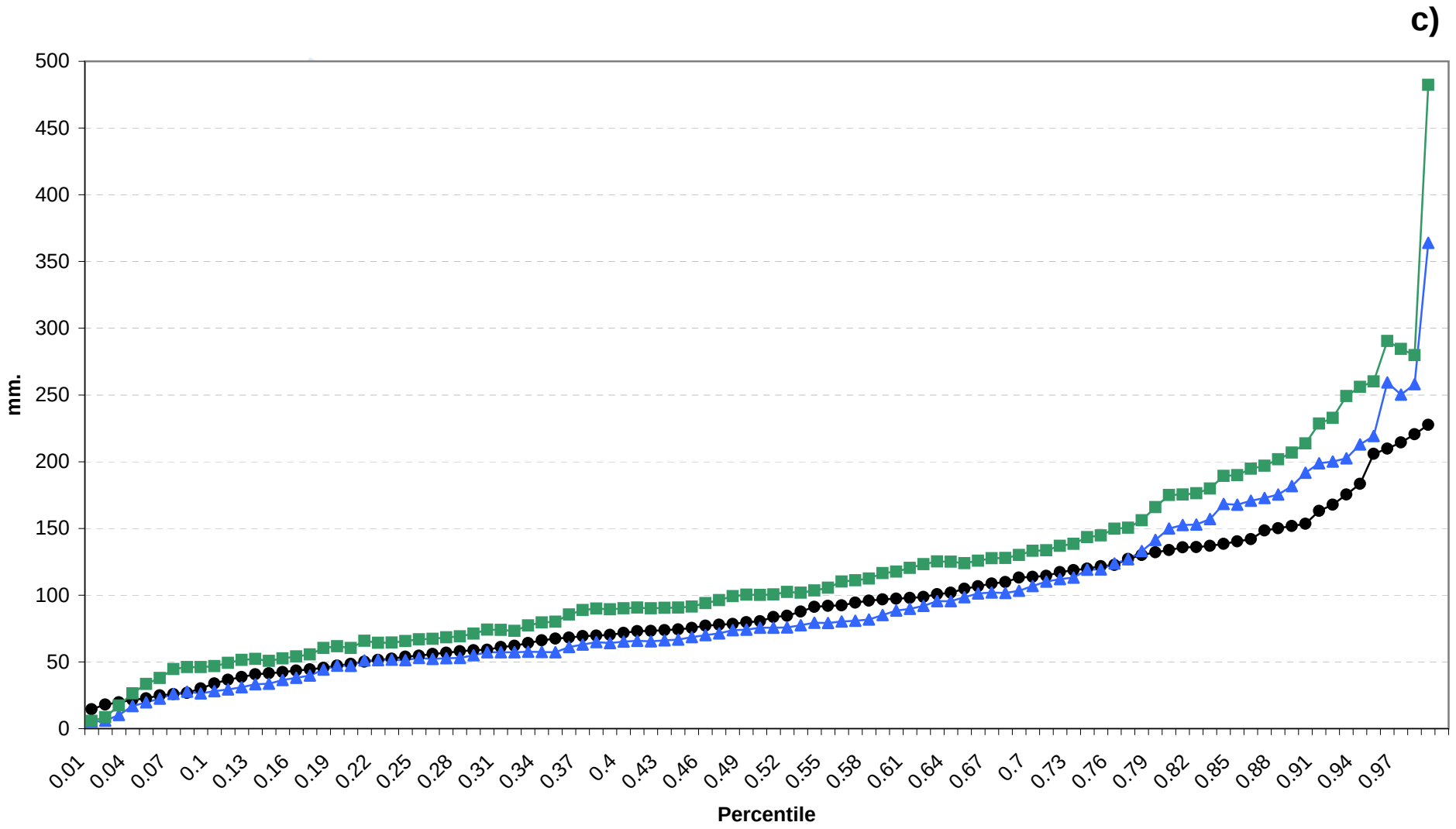
c)
500
450
400
350
300
250
200
150
100
50
0
mm.
0.01
0.04
0.07
0.1
0.13
0.16
0.19
0.22
0.25
0.28
0.31
0.34
0.37
0.4
0.43
0.46
0.49
0.52
0.55
0.58
0.61
0.64
0.67
0.7
0.73
0.76
0.79
0.82
0.85
0.88
0.91
0.94
0.97
Percentile

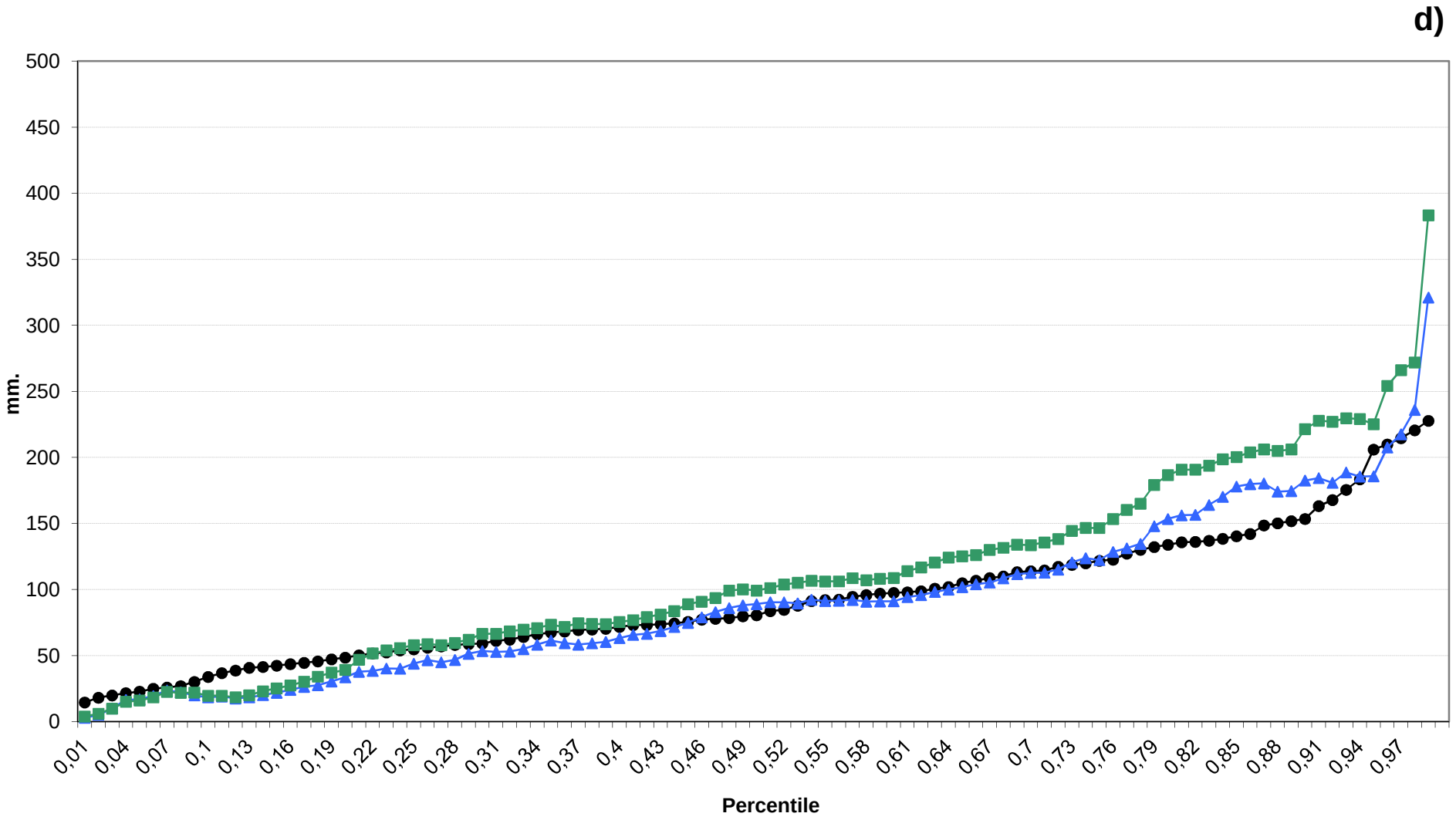

Figure 9: As in Figure 7, but for region R3.

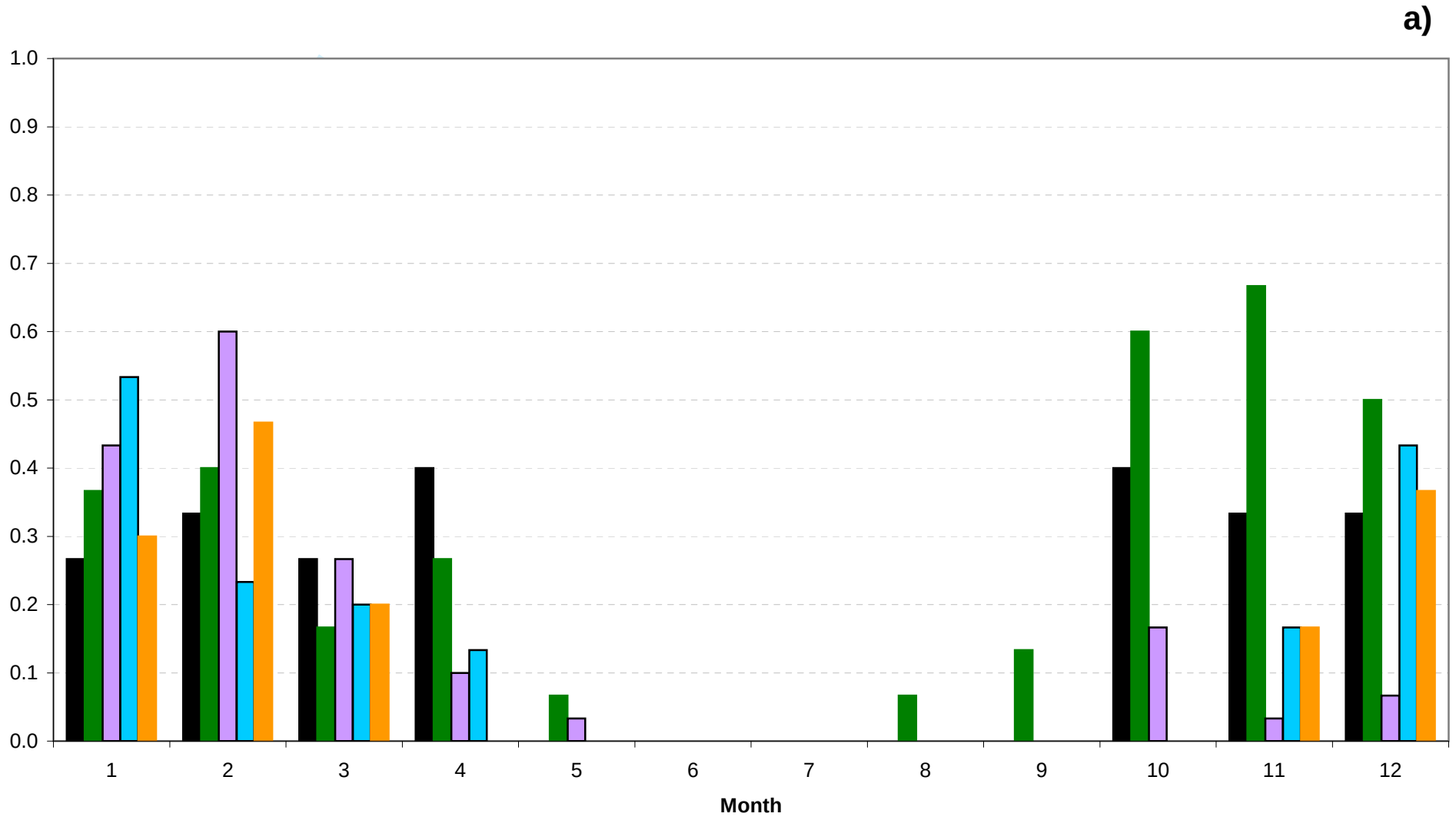
a)
1.0
0.9
0.8
0.7
0.6
0.5
0.4
0.3
0.2
0.1
0.0
1
2
3
4
5
6
7
8
9
10
11
12
Month

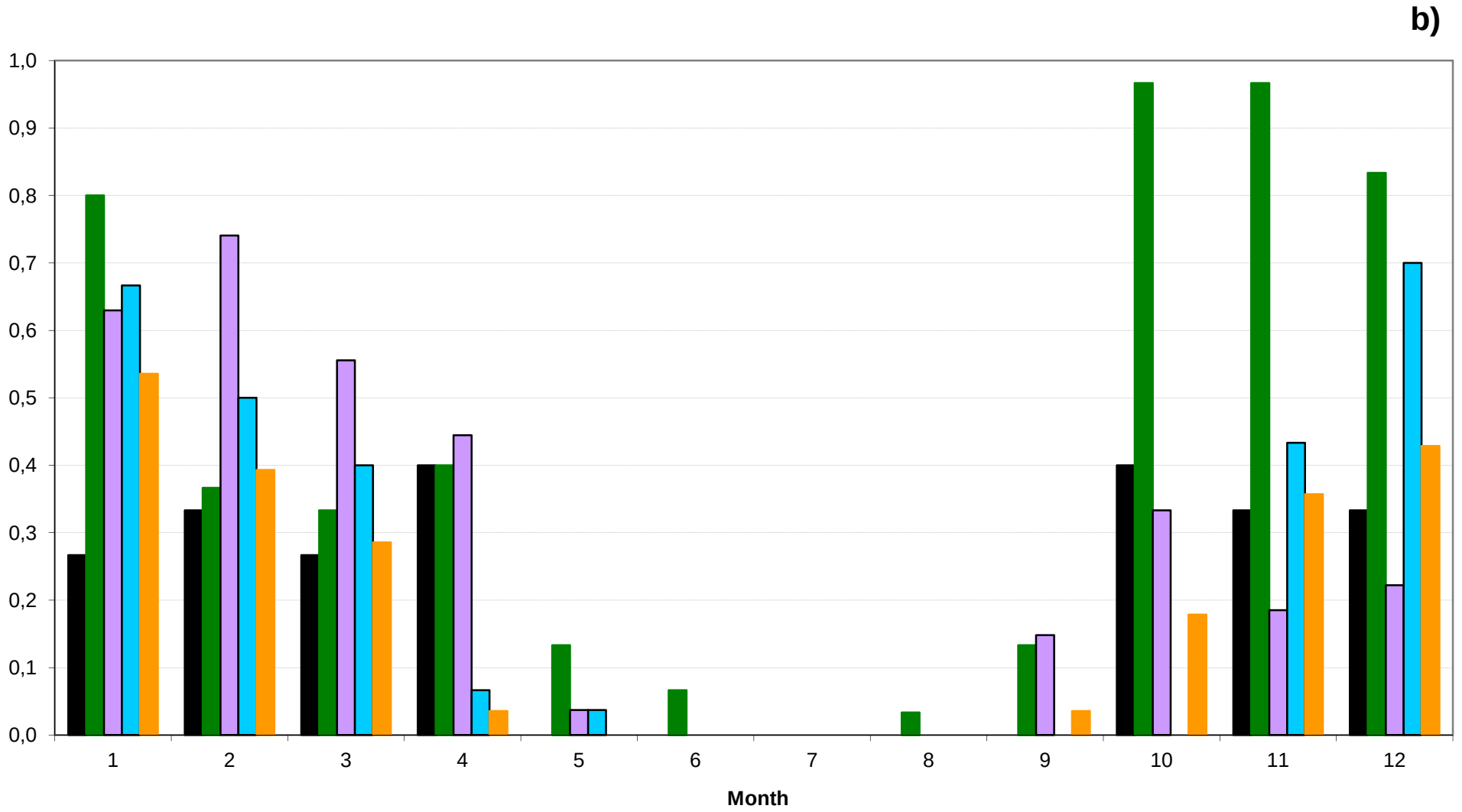

Figure 10: Annual cycle of the frequency of MEPs for region R1. Observed values 1990-2004 in black. Model projections for the near future in panel a) and for the end of the century in panel b), RCA in green, RegCM3 in violet, LMDZ in light blue and PROMES in orange.

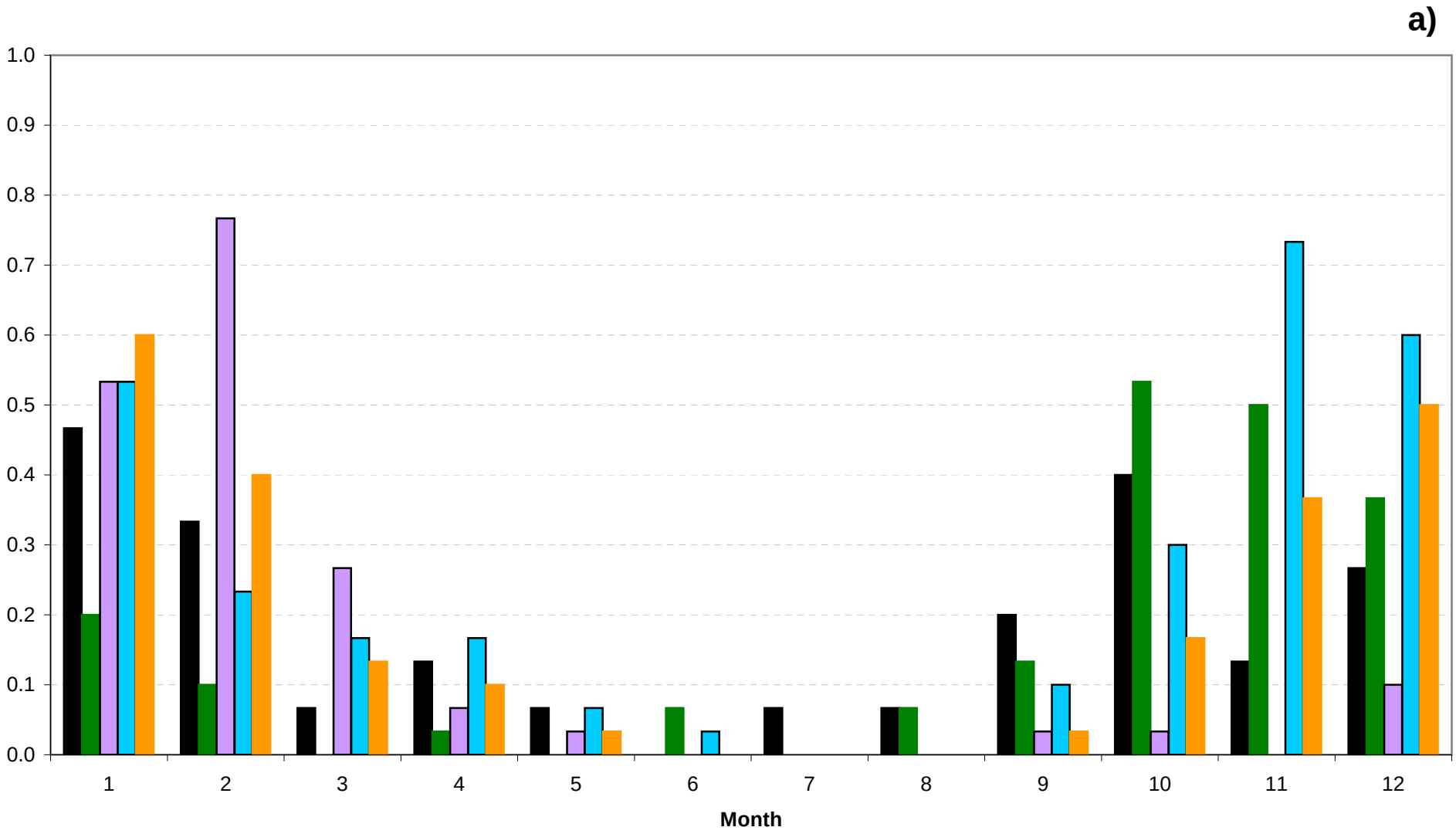
a)
1.0
0.9
0.8
0.7
0.6
0.5
0.4
0.3
0.2
0.1
0.0
1
2
3
4
5
6
7
8
9
10
11
12
Month

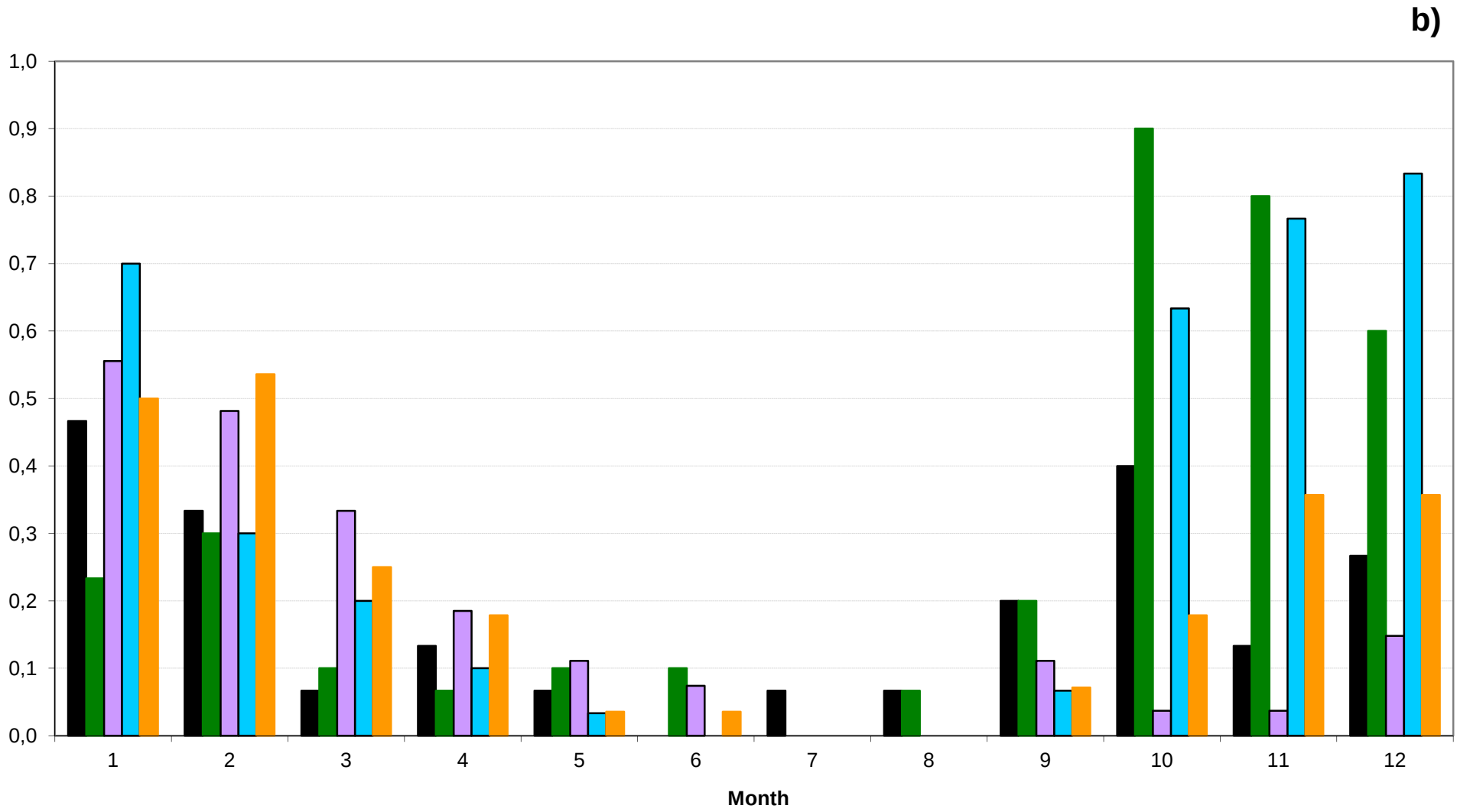

Figure 11: As in Figure 10, but for region R2.

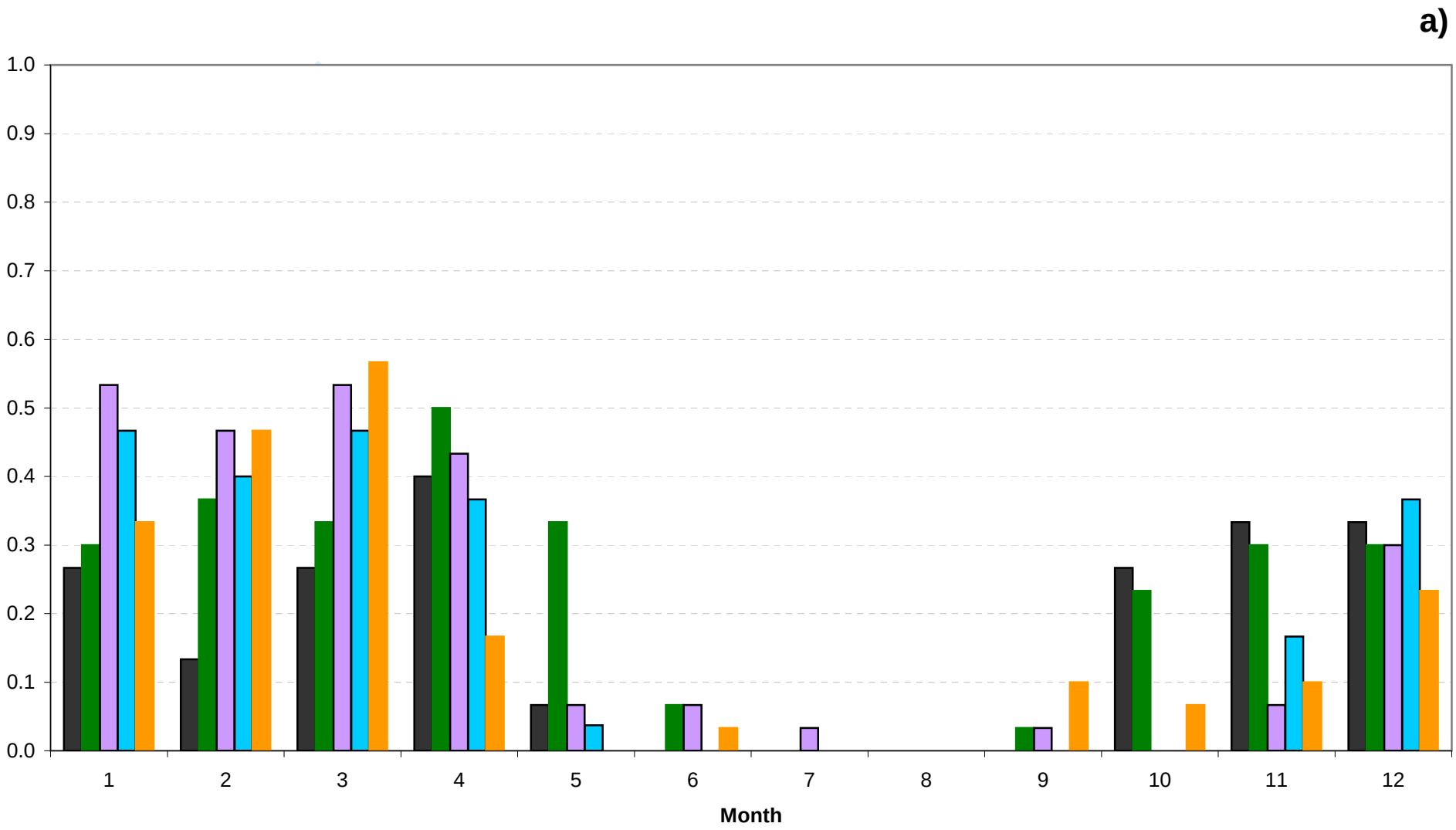
a)
1.0
0.9
0.8
0.7
0.6
0.5
0.4
0.3
0.2
0.1
0.0
1
2
3
4
5
6
7
8
9
10
11
12
Month

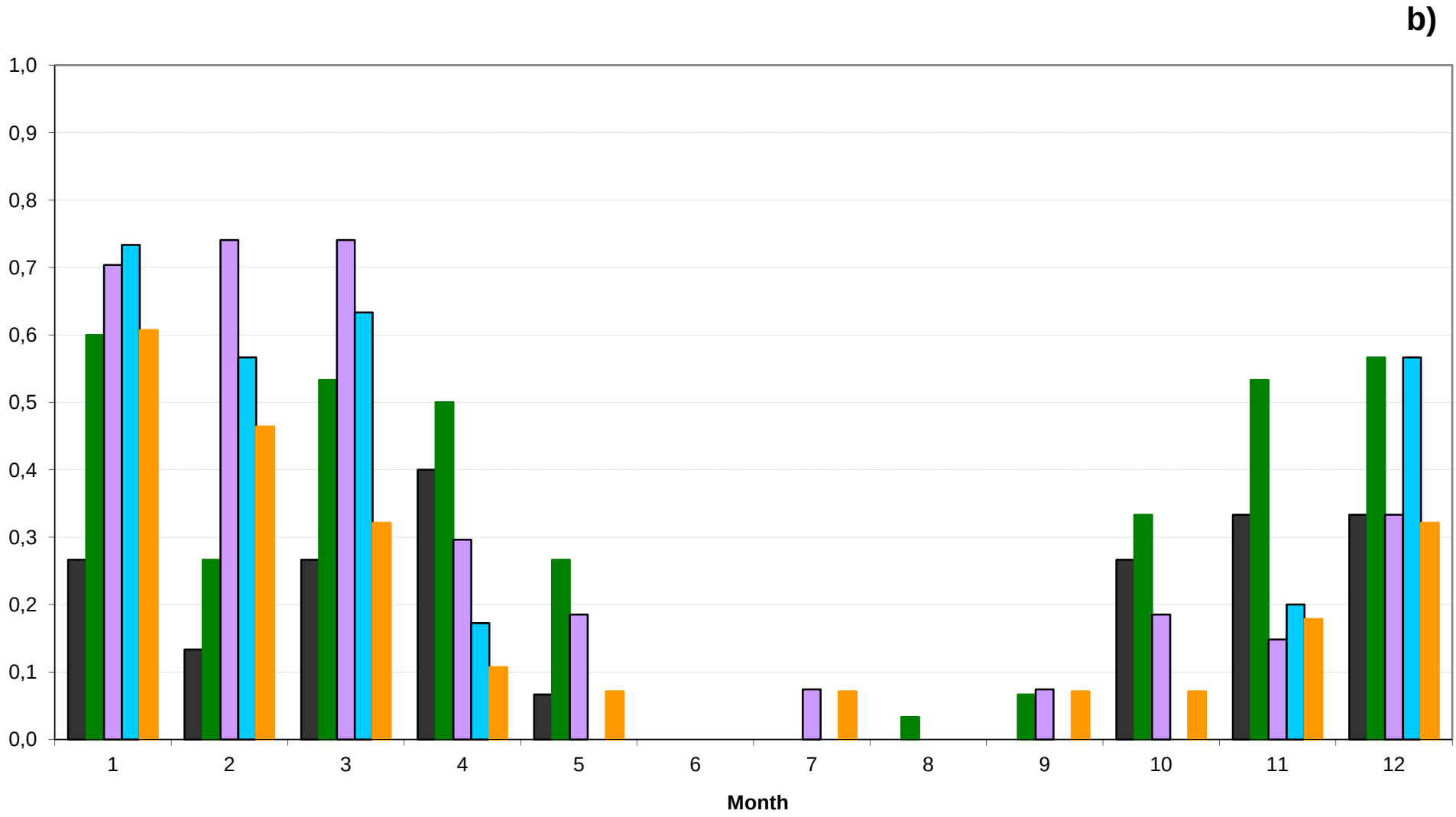

Figure 12: As in Figure 10, but for region R3.

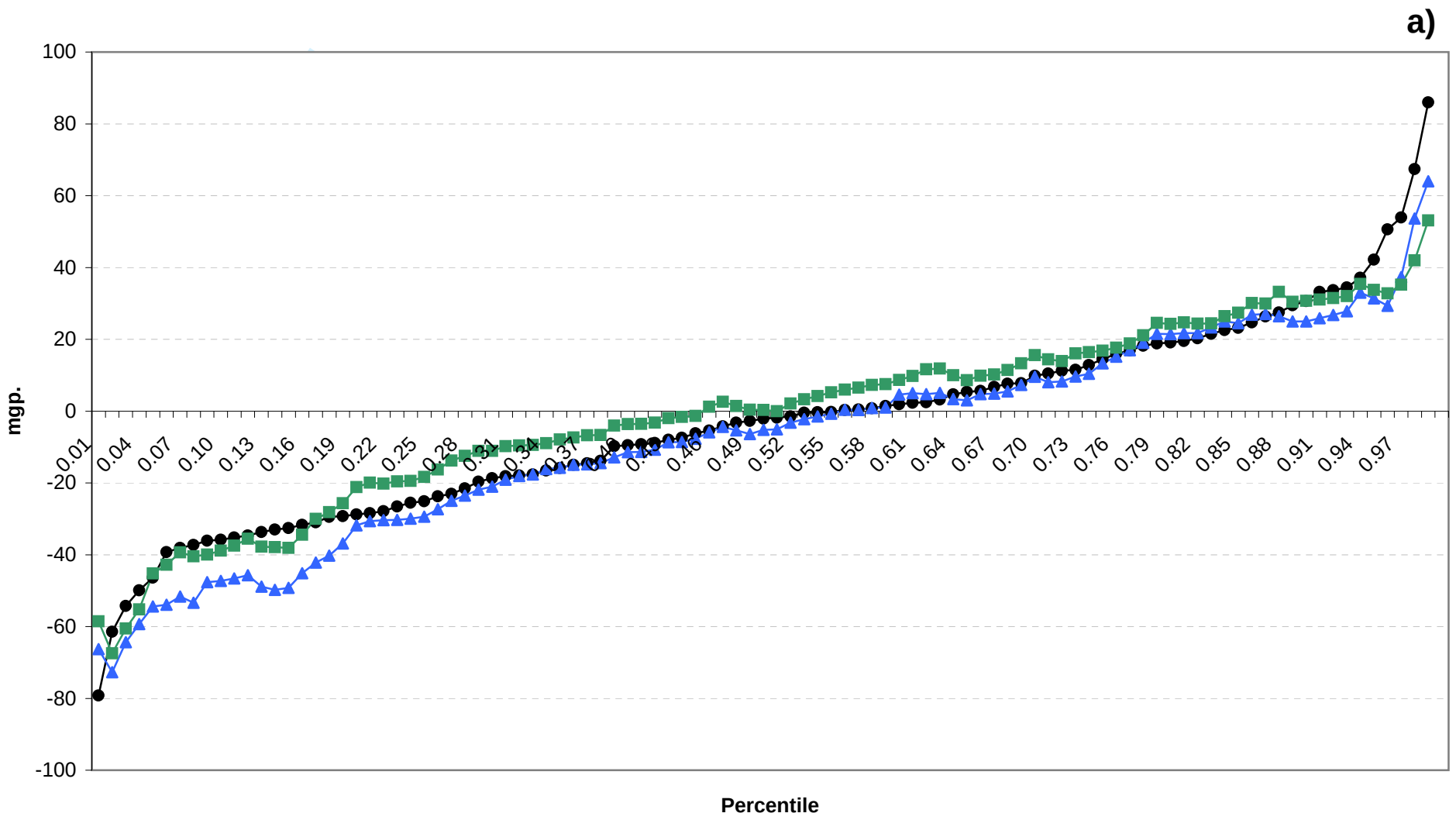
a)
100
80
60
40
20
0
-20
-40
-60
-80
-100
mgp.
0.01
0.04
0.07
0.10
0.13
0.16
0.19
0.22
0.25
0.28
0.31
0.34
0.37
0.40
0.43
0.46
0.49
0.52
0.55
0.58
0.61
0.64
0.67
0.70
0.73
0.76
0.79
0.82
0.85
0.88
0.91
0.94
0.97
Percentile

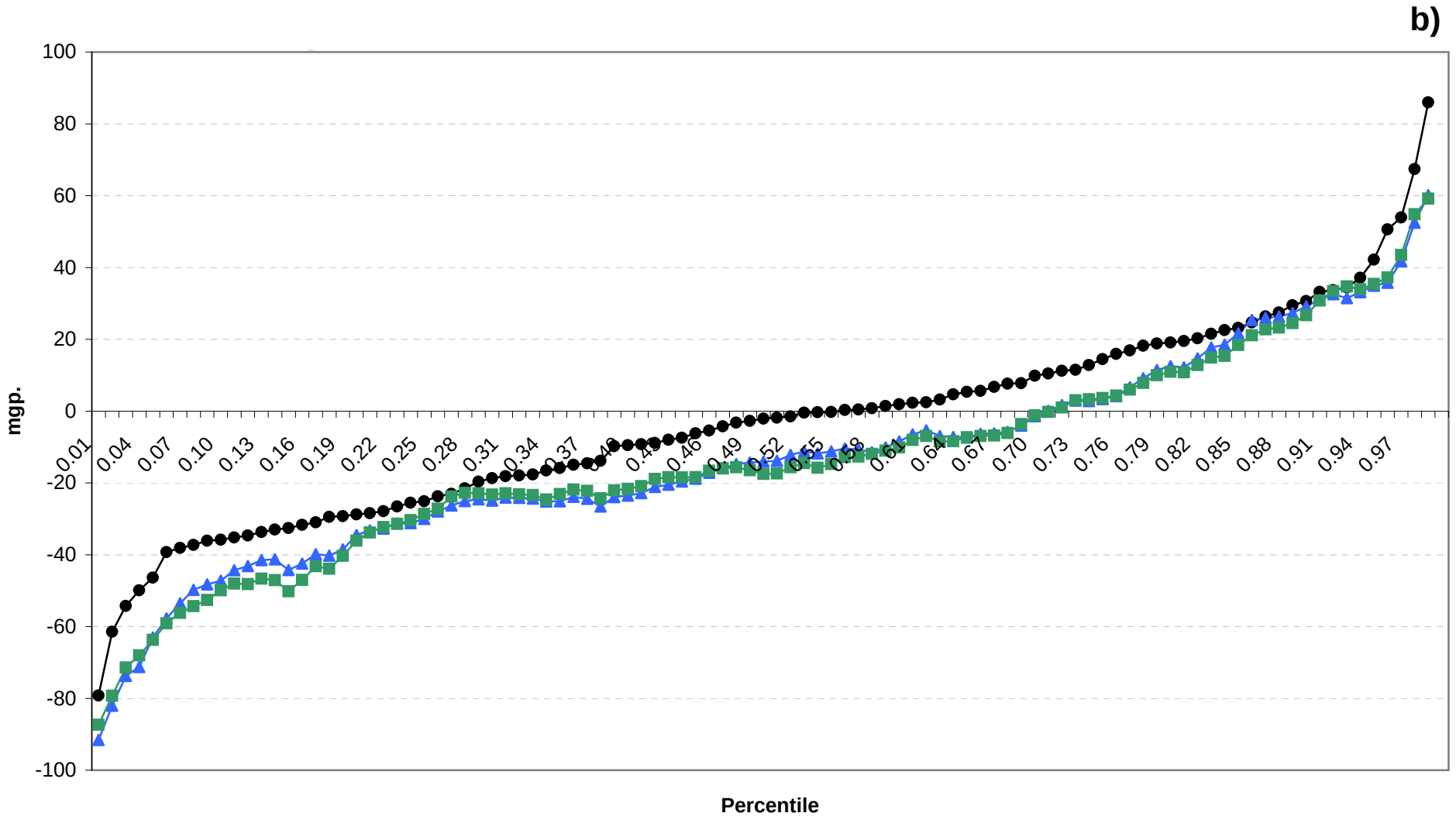
b)
100
80
60
40
20
0
-20
-40
-60
-80
-100
mgp.
0.01
0.04
0.07
0.10
0.13
0.16
0.19
0.22
0.25
0.28
0.31
0.34
0.37
0.40
0.43
0.46
0.49
0.52
0.55
0.58
0.61
0.64
0.67
0.70
0.73
0.76
0.79
0.82
0.85
0.88
0.91
0.94
0.97
Percentile

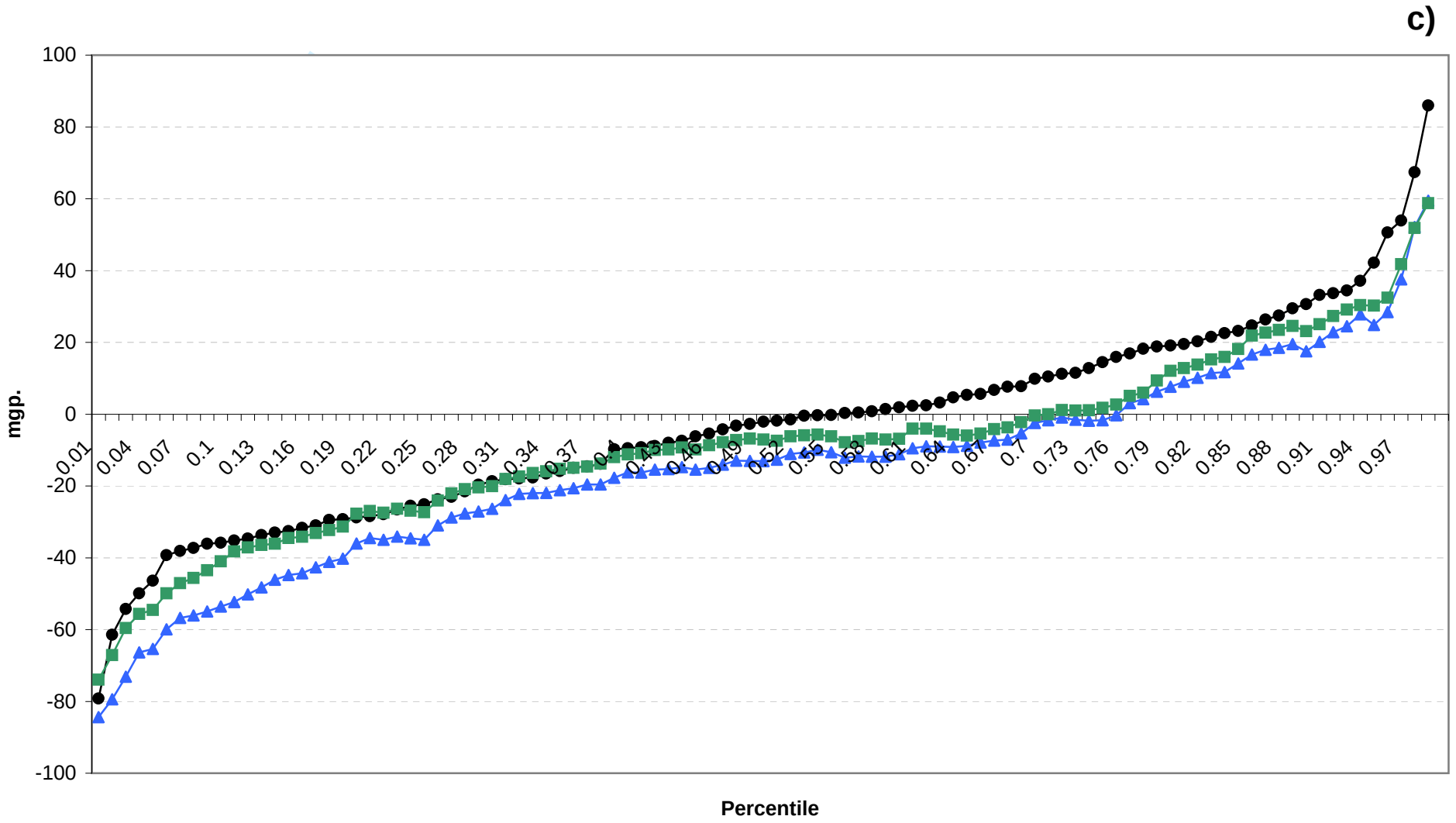
c)
100
80
60
40
20
0
-20
-40
-60
-80
-100
mgp.
0.01
0.04
0.07
0.1
0.13
0.16
0.19
0.22
0.25
0.28
0.31
0.34
0.37
0.4
0.43
0.46
0.49
0.52
0.55
0.58
0.61
0.64
0.67
0.7
0.73
0.76
0.79
0.82
0.85
0.88
0.91
0.94
0.97
Percentile

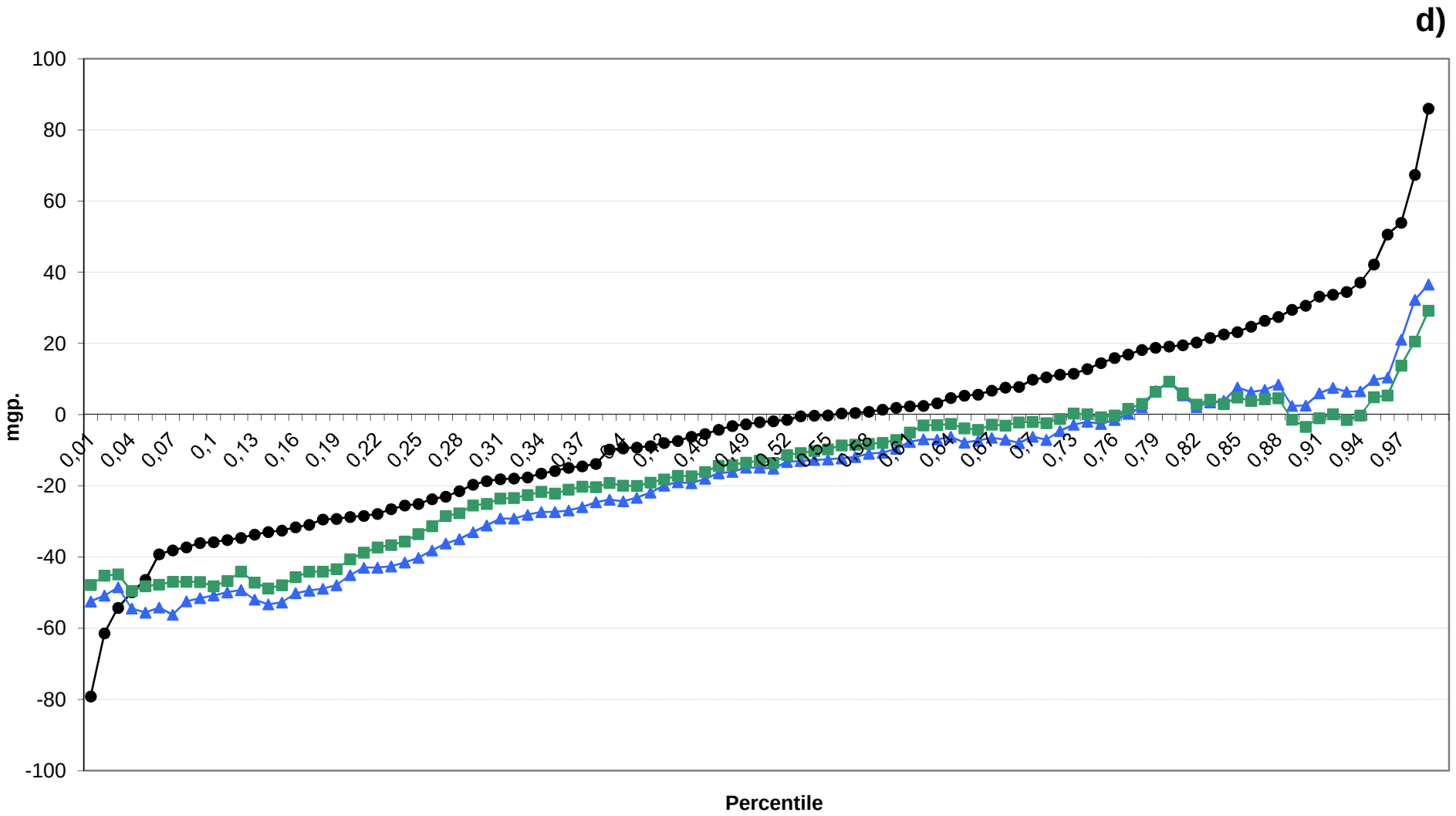

Figure 13: Percentile distribution of projected I500 index. a) RCA, b) PROMES, c) RegCM3, d) LMDZ for the near future (blue) and for the end of the century (green). In black the observed distribution for the 1990-2004 period.

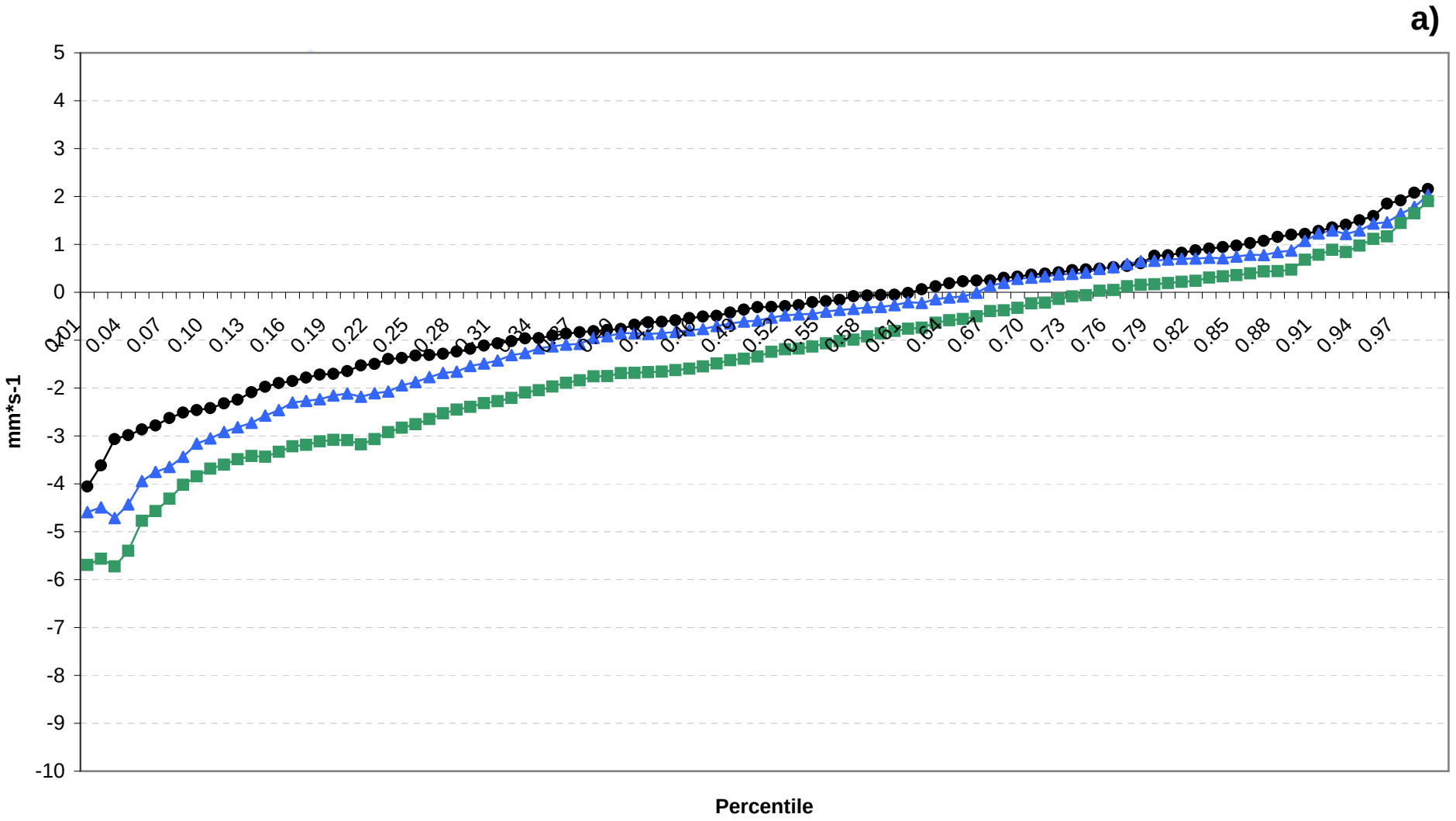
a)
5
4
3
2
1
0
-2
-3
-4
-5
-6
-7
-8
-9
-10
mm*s-1
0.01
0.04
0.07
0.10
0.13
0.16
0.19
0.22
0.25
0.28
0.31
0.34
0.37
0.40
0.43
0.46
0.49
0.52
0.55
0.58
0.61
0.64
0.67
0.70
0.73
0.76
0.79
0.82
0.85
0.88
0.91
0.94
0.97
Percentile

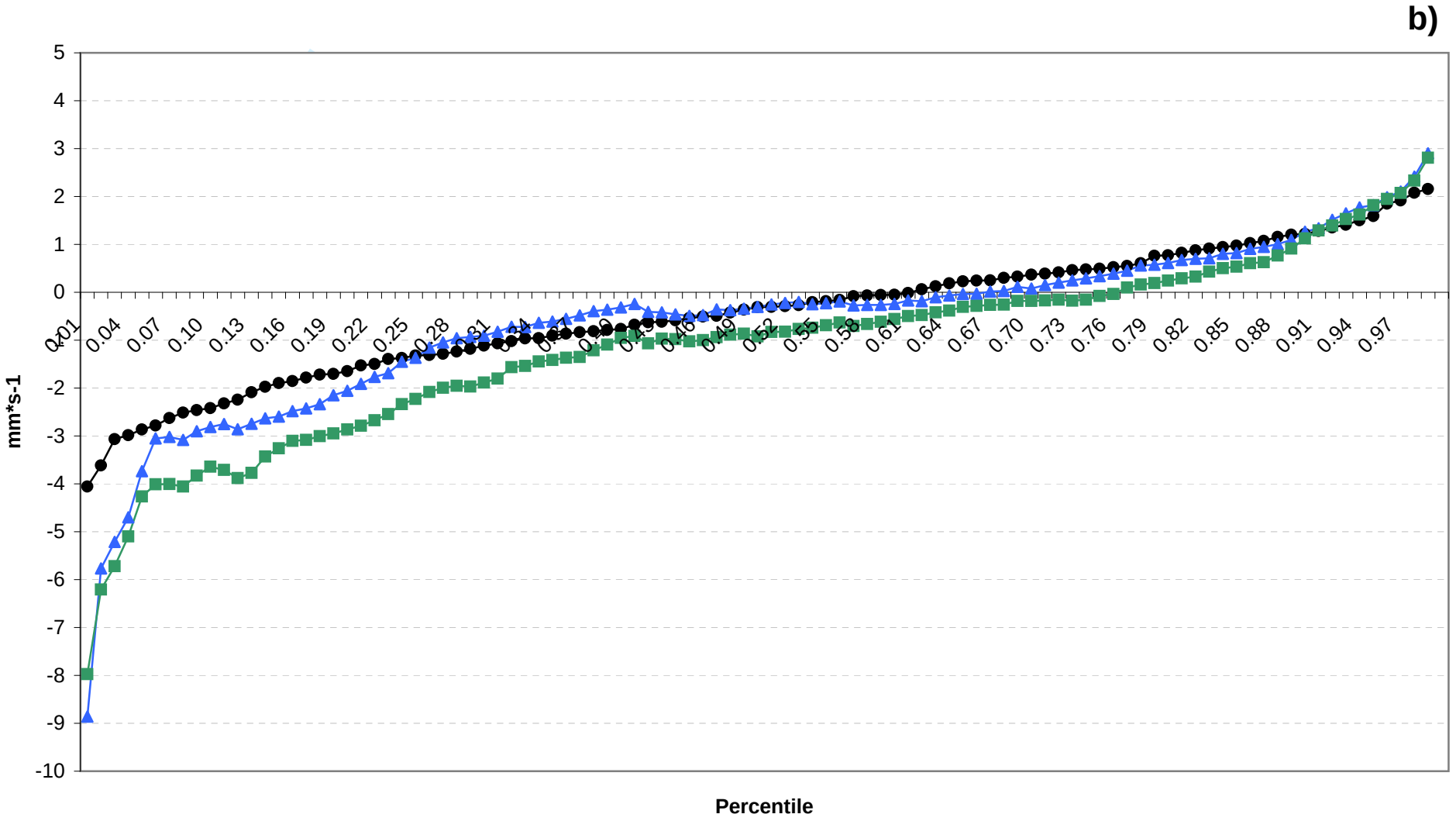
b)
5
4
3
2
1
0
-2
-3
-4
-5
-6
-7
-8
-9
-10
mm*s-1
0.01
0.04
0.07
0.10
0.13
0.16
0.19
0.22
0.25
0.28
0.31
0.34
0.37
0.40
0.43
0.46
0.49
0.52
0.55
0.58
0.61
0.64
0.67
0.70
0.73
0.76
0.79
0.82
0.85
0.88
0.91
0.94
0.97
Percentile

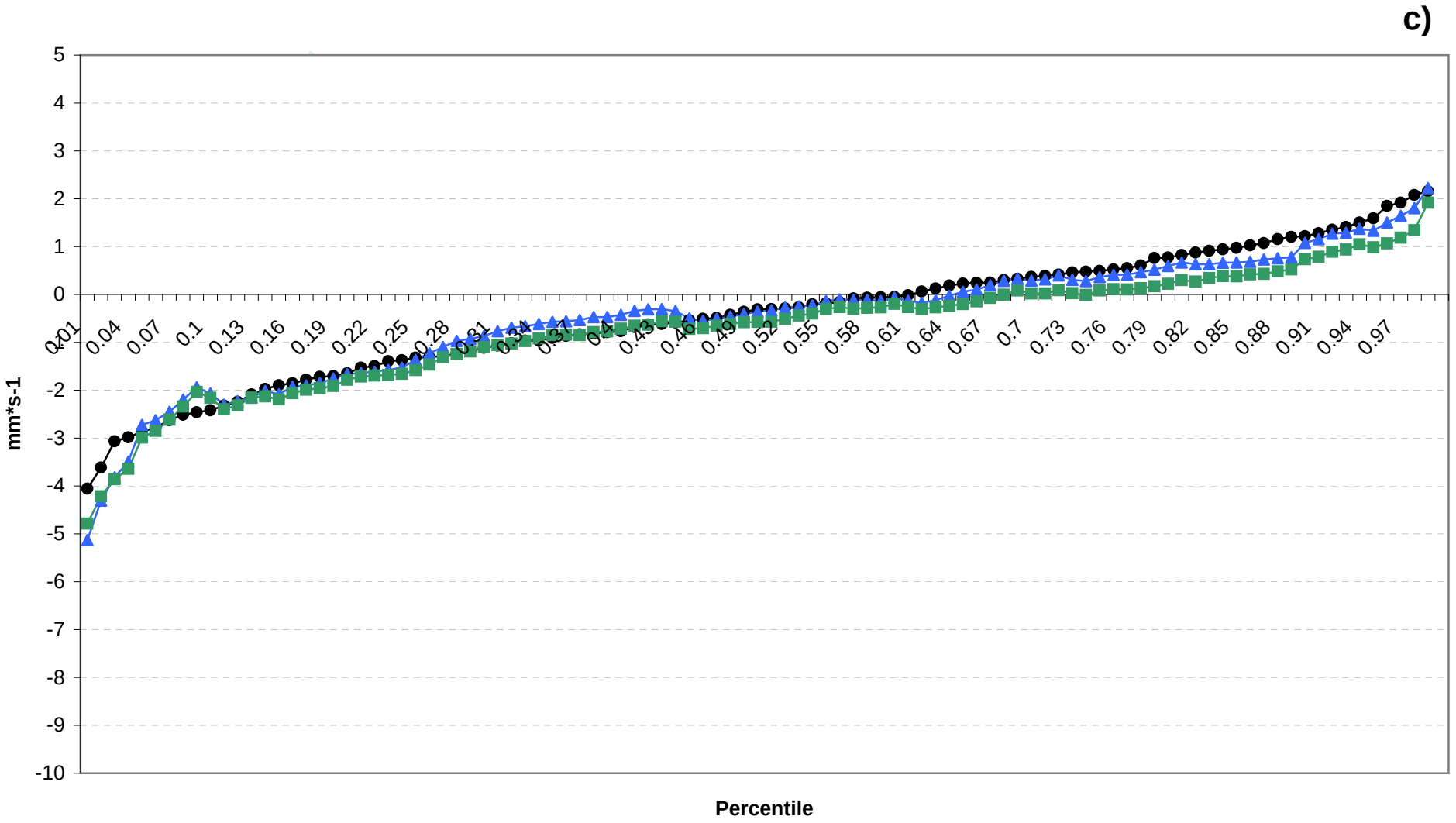
c)
5
4
3
2
1
0
-2
-3
-4
-5
-6
-7
-8
-9
-10
mm*s-1
0.01
0.04
0.07
0.1
0.13
0.16
0.19
0.22
0.25
0.28
0.31
0.34
0.37
0.4
0.43
0.46
0.49
0.52
0.55
0.58
0.61
0.64
0.67
0.7
0.73
0.76
0.79
0.82
0.85
0.88
0.91
0.94
0.97
Percentile

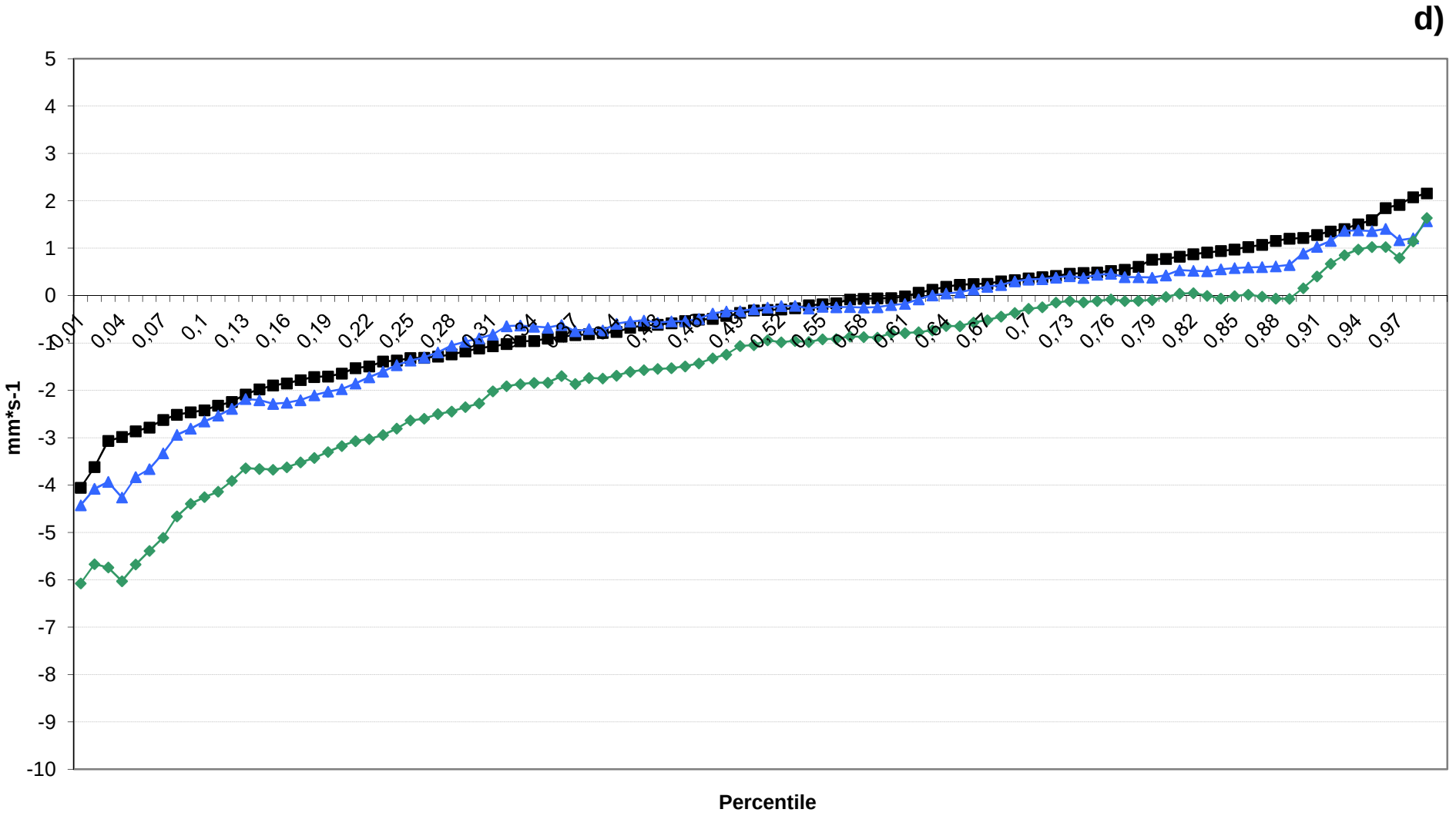

Figure 14: Percentile distribution of projected DE index. a) RCA, b) PROMES, c) RegCM3, d) LMDZ for the near future (blue) and for the end of the century (green). In black the observed distribution for the 1990-2004 period.